Industrial Compositional Streamline Simulation for Efficient and Accurate Prediction of Gas Injection Processes

Semi-Annual Report

Start date: April 1, 2006
End date: September 30, 2006

Principal Investigator: Margot Gerritsen

December 2006

DE-FC26-04NT15530-M001

Department of Petroleum Engineering
Stanford University
Green Earth Sciences Building
367 Panama Street
Stanford, CA 94305-2220

Disclaimer:
This report was prepared as an account of work sponsored by an agency of the United States Government. Neither the United States Government nor any agency thereof, nor any of their employees, makes any warranty, express or implied, or assumes any legal liability or responsibility for the accuracy, completeness, or usefulness of any information, apparatus, product, or process disclosed, or represents that its use would not infringe privately owned rights. Reference herein to any specific commercial product, process, or service by trade name, trademark, manufacturer, or otherwise does not necessarily constitute or imply its endorsement, recommendation, or favoring by the United States Government or any agency thereof. The views and opinions of authors expresses herein do no necessarily state or reflect those of the United States Government or any agency thereof.

Abstract

We are extending and improving our current Compositional Streamline Simulator (CSLS), which is being developed for the performance prediction of (near) miscible gas injection processes in heterogeneous reservoirs. This report covers the fourth six months of our two-year cooperative agreement. The report focuses on relaxation methods to solve for transport along streamlines. We have completed the research in this area. We continued our research on grid dependency issues, and have started porting our code to a shared memory SUN cluster, but will discuss these areas in a next report.

Table of Contents

List of graphical materials

1. Introduction

2. Executive Summary

   2.1. Personnel
   2.2. Important accomplishments

3. Experimental

4. Results and discussion

5. Conclusions

References

List of graphical materials

Figure 1: Fractional flow function $F_1(C_1)$. In the two-phase region, the function is S-shaped.

Figure 2: Derivative $\frac{dF_1}{dC_1}$ of the fractional flow function shown in figure 1.

Figure 3: Binary displacement – test case 1, pure light component (**d**) displaces pure heavy component (**a**).

Figure 4: Binary displacement - test case 2, mixture of two components (**h**) displaces pure component (**a**). The trailing shock has zero speed.

Figure 5: Ternary phase diagram - representation of a ternary composition on an equilateral triangle.

Figure 6: Tieline and non-tieline eigenvalues.

Figure 7: Tie-line and nontie-line paths for a ternary system with constant K-values. At equal eigenvalue points, the nontie-line path is tangent to tie-line path.

Figure 8: Solution path in the ternary phase diagram and saturation profile of the 3-component displacement.

Figure 9a: Results of upwind schemes on test case 1- binary displacement. N= 40, CFL = 0.35.

Figure 9b: Results of upwind schemes on test case 2- binary displacement. N= 40, CFL = 0.35. Here, the SPU needs about 200 grid points to resolve as accurately as TVD-RK2 or ENO-RK3.

Figure 10a: Results of component-wise application of upwind schemes on ternary displacement in the phase space. SPU is excessively diffusive. N= 80, CFL = 0.4.

Figure 10b: Solution profiles of ternary displacement got by component-wise application of upwind schemes. SPU smears the shocks and has a prominent dip in the zone-of-constant state. N= 80, CFL = 0.4.

Figure 11: A closer look at the TVD-RK2 and ENO-RK3 composition paths in the phase space, near the equal eigenvalue point. The path computed by the TVD-RK2 scheme jumps to an incorrect nontie-line near the equal eigenvalue point. N= 200, CFL = 0.4.

Figure 12: Comparison of 1st order Jin-Xin relaxation scheme and SPU. N= 40, CFL = 0.2.

Figure 13a: Phase space comparison of component-wise application of upwind schemes and 2nd order Jin-Xin relaxation scheme on ternary displacement. Composition path of Jin-Xin scheme is close to TVD-RK2 but has slightly more numerical diffusion than TVD-RK2. N= 80, CFL = 0.2.

Figure 13b: Solution profile of C_1 obtained by 2nd order Jin-Xin relaxation scheme is close to TVD-RK2. N= 80, CFL = 0.2.

Figure 14: A closer look at the 2nd order Jin-Xin scheme in the phase space near the equal eigenvalue point. The path computed by the Jin-Xin scheme behaves better than TVD-RK2 near the equal eigenvalue point but also has slightly more diffusion on the initial tie-line. N= 200, CFL = 0.2.

Figure 15a & 15b: Results of variable relaxation scheme on binary displacement. N= 40, CFL = 0.35. Variable relaxation scheme is less diffusive than Jin-Xin scheme and is quite close to SPU.

Figure 16a: Phase space comparison of ENO-RK3 and 2nd order variable relaxation scheme on ternary displacement. Composition path of the variable relaxation scheme is close to ENO-RK3. N= 80, CFL = 0.2.

Figure 16b: Comparison of solution profiles obtained by ENO-RK3 and 2nd order variable relaxation. N= 80, CFL = 0.2.

Figure 17: A closer look - 2nd order variable relaxation is close to ENO-RK3 and has much less diffusion than Jin-Xin scheme. It also behaves well near the equal eigenvalue point. N= 200, CFL = 0.2.

1. Introduction

Reliable prediction of the performance of miscible or near-miscible gas injection processes requires a simulation tool that can accurately predict both the local displacement efficiency and the global sweep. The local displacement efficiency is governed by pore-level interactions between the reservoir fluid and the injected fluid. Numerical methods used in compositional simulation must therefore accurately represent phase behavior. This means that a sufficiently high number of components is used to represent the oil and gas present, and that high order spatial discretizations must be employed instead of the commonly used first order upwind scheme (SPU). The global sweep depends primarily on the permeability field and gravity segregation. The highly mobile low viscosity gas will flow preferentially through high permeability flow paths, bypassing oil in less permeable areas of the reservoir. Thus, accurate prediction of global sweep requires detailed representations of heterogeneity and therefore a high grid density. As a result, the computational costs of compositional simulations can be very high.

Streamline simulation is an attractive approach to simulation these advection-dominated gas injection processes. We have developed a Compositional Streamline Simulator (CSLS) that shows promise for efficient and accurate performance prediction. In this project we are extending CSLS to include three-phase flow, and optimizing the simulator by developing and implementing an efficient grid adaptation procedure and code parallelization. This report presents results of the second half of the second year of this three-year project. Because this time period covers our summer quarter also, during which most of our students have internships, the report covers one research area only: relaxation methods.

2. Executive Summary

2.1. Personnel

The personnel in this 6-months period included Prof. Margot Gerritsen (PI), Prof. Lynn Orr (advisor), Dr. Jim Lambers (research associate) and Ms. Shalini Krishnamurthy and Mr. Jeremy Kozdon (PhD students).

Ms. Shalini Krishnamurthy is working on the development of error estimators to aid adaptation of the streamline grid and improve the current coverage algorithm. She is also exploring a novel numerical method based on relaxation schemes to handle the transport solve along streamlines.

Mr. Jeremy Kozdon has recently started a study on the grid orientation effect that may be encountered in gas injection processes. He is partly supported by the Center for Computational Earth and Environmental Sciences in the School of Earth Sciences at Stanford University.

Professor Lynn Orr is a project advisors contributing to the general planning and directing of the project.

We have hired a postdoctoral student, Henrik Loef, who will start his work with us November 1, 2006. Dr. Loef will be responsible for the porting of the CSLS code to a SUN shared memory system.

2.2. Important accomplishments

This report is succinct for two reasons. First, our postdoc did not yet commence work (he starts November 1, 2006). Second, one of our two students, Jeremy, took the period of June 1 through to September 15 to work with Chevron Energy Technologies on a summer internship. We will therefore only report on the work done by Shalini on relaxation methods.

2.2.1. Solving transport equations along streamlines: relaxations methods

Solving the transport equations along the streamlines is challenging due to strong non-linear coupling and weak hyperbolicity of the problems in phase space. Relaxation schemes aim to overcome these problems by reformulating the governing equations as a linear system of hyperbolic equations, with the specific intent of controlling hyperbolicity; the nonlinearity is restricted to the source term only. As we also discussed in our first semi-annual report, we are investigating whether these methods are useful in the context of miscible gas injection processes. They may provide a robust way to avoid problems with the loss of strict hyperbolicity commented on earlier. We have now completed this investigation.

For completeness, we have included the full discussion of relaxation methods and related schemes for solving hyperbolic systems of equations.

Relaxation schemes (Jin & Xin 1995) and central schemes (Nessyahu & Tadmor 1990, Kurganov & Tadmor 2000) avoid the use of nonlinear Riemann solvers and do not rely on the specific eigenstructure of the problem. Relaxation schemes overcome the dependency on Riemann solutions by solving an approximate problem, called the relaxation system, instead of solving the

original problem. The relaxation system replaces the original nonlinear and homogeneous conservation system with a linear hyperbolic system, with a stiff nonlinear source term.

As an example, consider the scalar conservation law

$$u_t + f(u)_x = 0,\ u(x,0) = u_0(x). \tag{1}$$

The relaxation system as proposed by Jin and Xin for Equation (1), takes the form

$$\begin{bmatrix} u \\ v \end{bmatrix}_t + \begin{bmatrix} 0 & 1 \\ a^2 & 0 \end{bmatrix} \begin{bmatrix} u \\ v \end{bmatrix}_x = \begin{bmatrix} 0 \\ -\frac{1}{\varepsilon}\left(v - f(u)\right) \end{bmatrix}, \tag{2}$$
$$u(x,0) = u_0(x),\ v(x,0) = f(u_0),$$

where the relaxation rate ε is a constant satisfying $0 < \varepsilon << 1$, and the parameter a, which is also a constant and referred to as the sub-characteristic speed, is chosen so that $-a < f'(u) < a$, $\forall u$, i.e. $a = \max\left|f'(u)\right|$.

The relaxation system approximates the original problem with a small dissipative correction controlled by ε. For ε sufficiently small, the original system is recovered. Numerically solving the relaxation formulation has one special advantage. Characteristic decomposition, though still the modus operandi, is now done on a linear hyperbolic structure with a full set of eigenvectors that is constant throughout the entire domain.

Although the relaxation system seems simpler to solve than the original nonlinear system, it now has a stiff source term, additional numerical diffusion and is twice as large as the original system. The stiff source term can be effectively handled by operator splitting (Jin 1995, LeVeque 2002), wherein the system is solved in two separate steps, an advection step, and an ODE step, as explained below. This introduces a splitting error, but it is of the order $O\left(\Delta t^r\right)$, where r is the number of RK stages used for time-stepping. The overhead of computing the additional unknown v can be avoided by resorting to sudden relaxation, i.e. simply setting $v = f(u)$ in the ODE step. The numerical diffusion however, depends on the magnitude of the sub-characteristic speed a. If the sub-characteristic speed is constant for the entire domain, as in the Jin-Xin scheme, the numerical diffusion will always be greater than that of the corresponding upwind schemes.

Governing equations

The phase compositions for 2-phase systems are often expressed in terms of equilibrium ratios (K-values), given for each component p by

$$K_p = \frac{c_{pV}}{c_{pL}} = \frac{\text{volume fraction of component } p \text{ in vapor phase}}{\text{volume fraction of component } p \text{ in liquid phase}}. \tag{3}$$

Generally the K-values are variable and computed as a part of the flashes. For our test cases we use systems with simplified phase behavior and assume that the K-values are constant. This assumption alters neither the nonlinear nature nor the weak hyperbolicity of the systems. The

phase viscosities can be computed by Lohrenz-Bray-Clark correlations (Lohrenz et al.1964). The viscosity ratio can also be assumed to be constant without altering the primary behavior. Volume occupied by a component can change as it transfers between the phases. Volume change on mixing does not change the character of the displacement; only the wave velocities change. Although in realistic settings volume change on mixing is taken into account, and is accounted for by a pressure correction after components are advected (Dindoruk 1982), we will ignore it here to simplify the mathematics and numerics.

To summarize, our simplifying assumptions are that

- the flow is advection dominated, that is, diffusion is negligible,
- the equilibrium ratios (K-values) are constant,
- the viscosity ratio between the two phases is fixed,
- the mixing is ideal, that is, volume change on mixing is negligible.

The conservation equations in 1D, with the above assumptions, are represented by,

$$\frac{\partial C_p}{\partial t} + \frac{\partial F_p}{\partial x} = 0 \text{, for } p = 1,2,\cdots n_c - 1 \tag{4}$$

where n_c is the number of components, C_p is the overall volume fraction of component p described by $C_p = c_{pV} S_V + c_{pL} S_L = c_{pV} S_V + c_{pL}(1 - S_V)$, c_{pV} and c_{pL} are the volume fractions of component p in vapor and liquid phases, S_V and S_L are the vapor and liquid saturations, F_p is the overall fractional volumetric flow of component p described by $F_p = c_{pV} f_V + c_{pL} f_L = c_{pV} f_V + c_{pL}(1 - f_V)$, and f_V and f_L are the vapor and liquid fractional flows. In the single phase region we have $F_p = C_p$. Henceforth we will drop the subscript on the vapor saturation and the fractional flow and represent them as S and f.

An additional constraint is that the volume fractions of each component must sum to 1, so we have

$$\sum_{p=1}^{n_c} C_p = 1, \ \sum_{p=1}^{n_c} c_{pV} = 1, \text{ and } \sum_{p=1}^{n_c} c_{pL} = 1. \tag{5}$$

The fractional flow function is given by

$$f = \frac{k_{rV}(S)(1 - k_{rL}(S) N_g \sin\theta)}{k_{rV}(S) + M k_{rL}(S)}, \tag{6}$$

where k_{rV} and k_{rL} are vapor and liquid relative phase permeabilities that depend on saturation S. We use quadratic permeabilities. N_g is the gravity number, θ is the dip angle and M is the constant viscosity ratio. A typical fractional flow function for horizontal flow $(\theta = 0)$, using

quadratic relative permeabilities, assuming zero residual liquid saturation, and assuming zero critical vapor saturation looks like

$$f = \begin{cases} \dfrac{S^2}{S^2 + M(1-S)^2} & \text{in two phase region,} \\ 1 & \text{in vapor phase,} \\ 0 & \text{in liquid phase.} \end{cases} \tag{7}$$

Two-component displacements

At the simplest level we have two component (binary) displacements, where a light gas displaces a heavy hydrocarbon. This is a generalization of displacement of oil by water, the Buckley-Leverett problem (Lake 1989). Studying two-component displacement is useful because the solution to the two-component problem reappears as segments of the solution in systems with more components. We use the binary problem to analyze the behavior of the relaxation schemes. Since this is a scalar conservation law we do not have points of weak hyperbolicity.

The governing equation for binary displacement, given in terms of the injected component is

$$\frac{\partial C_1}{\partial t} + \frac{\partial F_1}{\partial x} = 0 \ , \tag{8}$$

with the initial condition $C_1(x,0) = \begin{cases} C_1^J \text{ if } x < 0 \\ C_1^I \text{ if } x > 0 \end{cases}$,

where C_1 and F_1 are described as $C_1 = c_{1V} S + c_{1L}(1-S)$, $F_1 = c_{1V} f(S) + c_{1L}(1 - f(S))$, and $f(S)$ as given in Equation (7) .

Note that for the Buckley-Leverett problem, each component exits only in one phase, and hence the volume fraction of the displaced component and the fractional flow reduce to $C_1 = c_{1V} S$, $F_1 = c_{1V} f(S)$, respectively, and the governing equation becomes $\frac{\partial S}{\partial t} + \frac{\partial f}{\partial x} = 0$. Figures 1 and 2 show the fractional flow curve and the propagation velocity for the binary displacement problem. In the single phase regions, $F_1 = C_1$. In the two-phase region, the curve is S-shaped, similar to the Buckley-Leverett flow curve.

We look at the solution profiles of two test cases shown in Figures 3 and 4. In the first case, a pure light component (point **d** on the fractional flow curve) displaces a pure heavy component (point **a**). The solution for the first case, shown in Figure 3, consists of a leading shock, a spreading wave and a trailing shock. In the second case, a mixture of two components (located by the point **h** on the flow curve) displaces the pure component (point **a**). The solution, depicted in Figure 4, has a leading shock with unit velocity and a trailing shock with zero velocity. The zone between the two shocks is called a zone of constant state. Here the composition remains constant (point **i**) but has two velocities, the leading shock velocity and the trailing shock velocity.

Ternary systems

For ternary systems, in addition to the composition profiles, we also study the ternary phase diagrams to obtain more information about the phase behavior of the compositions. Ternary phase diagrams represent the component concentrations of all possible mixtures of the three components in a two-dimensional space. Because the volume fractions of the three components sum to one, the phase compositions can be conveniently represented on an equilateral triangle (Lake 1989). Each vertex represents 100% of the component associated with that vertex, and the opposite vertex 0% (Figure 5). Each point within the triangle represents a mixture of the three components; the volume fractions are read from the perpendicular distance from that point to the three sides of the triangle. For gas/oil systems, the component associated with the top vertex of the triangle is usually the lightest, and the component associated with the bottom left vertex is usually the heaviest.

The conservation equations for 3-component nonlinear systems are given by

$$\frac{\partial C_1}{\partial t}+\frac{\partial F_1}{\partial x}=0, \qquad (9)$$
$$\frac{\partial C_2}{\partial t}+\frac{\partial F_2}{\partial x}=0,$$

with the initial condition $C_p(x,0)=\begin{cases} C_p^J \text{ if } x<0 \\ C_p^I \text{ if } x>0 \end{cases}$ for $p=1,2$ and with

$$C_1=c_{1V}S+c_{1L}(1-S), \qquad C_2=c_{2V}S+c_{2L}(1-S),$$
$$F_1=c_{1V}f(S)+c_{1L}(1-f(S)), \qquad F_2=c_{2V}f(S)+c_{2L}(1-f(S)),$$

and $f(S)$ as given in (7) .

This system has two eigenvalues given by (Figure 6)

$$\lambda_{\mathrm{t}}=\frac{\partial F_1}{\partial C_1}=\begin{cases} \frac{df}{dS} & \text{in the two phase region,} \\ 1 & \text{in the single phase region,} \end{cases} \qquad (10a)$$

and

$$\lambda_{\mathrm{nt}}=\frac{F_1+q}{C_1+q}, \text{ with } q=\frac{c_{1L}^2}{\gamma(K_1,K_2,K_3)}. \qquad (10b)$$

The corresponding eigenvectors are

$$\vec{e}_{\mathrm{t}}=\begin{bmatrix}1\\0\end{bmatrix} \text{ and } \vec{e}_{\mathrm{nt}}=\begin{bmatrix}1\\ \dfrac{\lambda_{\mathrm{t}}-\lambda_{\mathrm{nt}}}{\frac{\partial F_1}{\partial c_{1L}}}\end{bmatrix}. \qquad (11)$$

The eigenvectors correspond to the possible paths a solution can trace in the phase space. The eigenvector $\vec{e}_t$ corresponds to the straight line paths in the phase space, known as the *tie-line*

paths (Figure 7). The eigenvector $\vec{e}_{nt}$ corresponds to the curved paths in the phase space, known as the *nontie-line* paths. Within the two-phase region only certain specific volume fractions of liquid and vapor phase (c_{pL} and c_{pV}) can be in equilibrium, and the tie-lines connect these equilibrium volume fractions. So, on a given tie-line, c_{pV} and c_{pL} remain constant for all the components. Tie-lines also connect the vapor locus and the liquid locus in the phase space. The point at which a tie-line intersects the vapor locus has $S_V = 1$ and $S_L = 0$; the point where it intersects the liquid locus has $S_V = 0$ and $S_L = 1$. Nontie-line paths connect the various tie-lines. When the eigenvalues $\lambda_t = \lambda_{nt}$, the eigenvectors $\vec{e}_t = \vec{e}_{nt}$, the system has dependent eigenvectors, and hence is no longer diagonalizable. That is, the system becomes weakly hyperbolic and any numerical method which depends on the existence of a full set of independent eigenvectors may not perform well at such points. This behavior is only for systems with two phases; with three-phase systems we encounter elliptic regions instead (Juanes & Patzek 2004).

The solution to the ternary problem looks like a combination of two binary displacements. Consider the test case shown in Figure 8, which illustrates the salient features of a ternary problem. There are two key tie-lines, one extending through the initial oil (point **a**), and another extending through the injection gas (point **f**). In the two-component case, the entire displacement occurs on a single tie-line. Hence on each tie-line of the ternary system the solution has, like a binary solution, a shock and a rarefaction. As gas is injected, there are two transitions from the single-phase region to the two-phase region: a leading shock (**a-b**) on the initial tie-line, and a trailing shock (**e-f**) on the injection tie-line. Inside the two-phase region there is a small rarefaction (**b-c**), as the composition varies along the initial tie-line. At the point (**c**), the initial tie-line is tangential to a nontie-line curve. Here, the eigenvalues and the eigenvectors coincide, and the system becomes weakly hyperbolic. The composition then traces the nontie-line path as a rarefaction (**c-d**). At point **d** the solution encounters the injection tie-line, where the velocity jumps from the nontie-line eigenvalue λ_{nt} to the tie-line eigenvalue λ_t. The composition remains constant at **d** for the entire jump, forming a zone of constant state. On the injection tie-line there is one more rarefaction (**d-e**) which connects to the trailing shock (**e-f**).

In practical settings the initial and injection conditions are rarely constant, and the problem has to be solved numerically. In a component-wise numerical method with a constant grid spacing $\Delta x = \Delta x_j = \left(x_{j+\frac{1}{2}} - x_{j-\frac{1}{2}}\right)$, and a time-step Δt, we update the solution in the jth cell, at time level *n+1*, according to

1. Set $\mathbf{C}_j^{n+1} = \mathbf{C}_j^n - \dfrac{\Delta t}{\Delta x}\left[\mathbf{F}_{j+\frac{1}{2}}^n - \mathbf{F}_{j-\frac{1}{2}}^n\right]$, where $\mathbf{C} = \lfloor C_1, C_2 \ldots C_{n_c} \rfloor$ and $\mathbf{F} = \lfloor F_1, F_2 \ldots F_{n_c} \rfloor$,
2. Iteratively solve the nonlinear set of equations-of-state to obtain S_j^{n+1} (the most expensive step),
3. Compute $f_j^{n+1}, \mathbf{F}_j^{n+1}, \mathbf{F}_{j+\frac{1}{2}}^{n+1}$ using the newly computed S_j^{n+1}.

Figures 9a and 9b show the results of upwind schemes on the two-component displacements. The excessive numerical diffusion of the first order upwind scheme, which is also called the Single Point Upstream weighting scheme (SPU), is more apparent in the leading shock of the second example. SPU requires about 200 grid cells to obtain the same resolution as TVD-RK2 or ENO-RK3 scheme with 40 grid cells. At lower speeds, the numerical diffusion of the upwind schemes

decreases. For example 2, where a mixture of components is injected, the trailing shock has zero speed and the upwind schemes resolve the trailing shock with almost no smearing.

With the ternary system, the numerical diffusion of the first order scheme not only smoothes the shocks, but also seems to cause errors in the shock speeds. This can be explained by observing the discrepancy between the computed compositional path and the MOC path in the phase space. The numerical diffusion pulls the computed path away from the MOC path, thus altering the speeds of the computed solution. This error mimics the behavior of the system in the presence of physical diffusion. The nonlinear system can also introduce other errors not seen in the scalar two-component problem. For example, the solution may show a dip in the zone of constant state, in other words, too much oil is left behind. This error is frequently seen with nonlinear systems when a discontinuity is present in the initial data and occurs due to the fact that the Hugoniot locus for the nonlinear systems is not a straight line as it is in the scalar case (LeVeque 2002). If MOC is used to compute the solution up to a small time t_1, and this solution is used as the initial state for the numerical scheme, there is a clear reduction in the error at zone of constant state. Though we do not see it in the relatively simple test cases here, component-wise application of upwind schemes may also increase or introduce errors (Qiu & Shu 2002).

Higher order schemes (second order TVD-RK2 and third order ENO-RK3) contain much less numerical diffusion than the first order scheme (Figures 10a and 10b). The shocks are captured more accurately and the error in the zone of constant state is reduced. The solution path in phase space is also closer to the MOC path. Figure 11 gives a closer look at the numerical composition paths in phase space near the equal eigenvalue point. The numerical path computed by the TVD-RK2 scheme jumps from the initial tie-line to an incorrect nontie-line near the equal eigenvalue point. This path is different from the path that would have been traced in the presence of physical diffusion. This error is observed when grids are refined and there is very little numerical diffusion in the scheme. ENO-RK3 behaves better at the equal eigenvalue point.

The improved accuracy of the higher order schemes comes with a price of increased computational cost per time step. For every RK stage introduced in order to maintain a higher temporal accuracy, an additional flash is required. TVD-RK2 requires two flashes per time step and ENO-RK3 requires three flashes per time step. But since the higher order methods allow the usage of coarser grids, these schemes are more efficient than the first order scheme.

Jin-Xin relaxation

The Jin-Xin relaxation scheme replaces the original system of conservation laws (Equation 4) by

$$\frac{\partial \mathbf{C}}{\partial t} + \frac{\partial \mathbf{V}}{\partial x} = 0, \quad \mathbf{C}, \mathbf{V} \in \mathbf{R}^{n_c - 1}, \tag{12}$$

$$\frac{\partial \mathbf{V}}{\partial t} + \mathbf{A}^2 \frac{\partial \mathbf{C}}{\partial x} = \frac{1}{\varepsilon}(\mathbf{F}(\mathbf{C}) - \mathbf{V}), \quad \text{with } 0 < \varepsilon << 1,$$

$$\mathbf{C} = \left[C_1, C_2 \ldots C_{n_c-1}\right]^{\mathrm{T}}, \text{ and } \mathbf{V} = \left[V_1, V_2 \ldots V_{n_c-1}\right]^{\mathrm{T}},$$

with the initial conditions $\mathbf{C}(x,0) = \begin{cases} \mathbf{C}^J \text{ if } x < 0 \\ \mathbf{C}^I \text{ if } x > 0 \end{cases}$, and $\mathbf{V}(x,0) = \mathbf{F}(\mathbf{C}(x,0))$.

Here $\mathbf{A}$ is a positive diagonal matrix given by, $\mathbf{A} = diag(a_1, a_2 \cdots a_{n_c-1})$, where the diagonal elements $\{a_p\}$ are the so-called sub-characteristic speeds. We refer to the parameter ε as the relaxation rate. In the limit $\varepsilon \to 0$, $\mathbf{V} \to \mathbf{F}(\mathbf{C})$ and the relaxation system (Equation 12) reduces to the original conservation law (Equation 4). Using a Chapman-Enskog expansion (Chapman and Cowling 1970) to represent $\mathbf{V}$, the relaxation system can be seen as an approximation to the original conservation law with a small dissipative correction. The Chapman-Enskog expansion

$$\mathbf{V}(x,t) = \mathbf{F}(\mathbf{C}(x,t)) + \varepsilon\, \mathbf{V}_1(x,t) + \varepsilon^2\, \mathbf{V}_2(x,t) + \varepsilon^3\, \mathbf{V}_3(x,t) + \cdots , \tag{13}$$

is motivated by the fact that $\mathbf{V} \to \mathbf{F}(\mathbf{C})$ for small ε.

Substituting this expansion for $\mathbf{V}$ in Equation (12), the first order approximation to the relaxation system becomes

$$\frac{\partial \mathbf{C}}{\partial t} + \frac{\partial \mathbf{F(C)}}{\partial x} = \varepsilon \frac{\partial}{\partial x}\left((\mathbf{A}^2 - \mathbf{F}'(\mathbf{C})^2) \frac{\partial \mathbf{C}}{\partial x} \right) + \mathrm{O}(\varepsilon^2), \tag{14}$$

where $\mathbf{F}'(\mathbf{C})$ is the Jacobian of the flux function $\mathbf{F(C)}$.

In Equation (14), $\varepsilon \frac{\partial}{\partial x}\left((\mathbf{A}^2 - \mathbf{F}'(\mathbf{C})^2) \frac{\partial \mathbf{C}}{\partial x} \right)$ is a $\mathrm{O}(\varepsilon)$ dissipative term, with $\varepsilon(\mathbf{A}^2 - \mathbf{F}'(\mathbf{C})^2)$ being the diffusion coefficient matrix. Equation (14) is well-posed only if $(\mathbf{A}^2 - \mathbf{F}'(\mathbf{C})^2)$ is positive semi-definite for all $\mathbf{C}$. This requirement on the diffusion coefficient matrix $(\mathbf{A}^2 - \mathbf{F}'(\mathbf{C})^2)$ of the relaxation system is called the sub-characteristic condition. In 1D, it is equivalent to

$$\lambda^2 \le a^2, \quad \text{where} \quad \lambda = \max_{1 \le p \le n_c - 1} |\lambda_p| \quad \text{and} \quad a = \min_{1 \le p \le n_c - 1} a_p, \tag{15}$$

where λ_p are the eigenvalues of the Jacobian $\mathbf{F}'(\mathbf{C})$.

For $\mathbf{C}$ in a bounded domain, the sub-characteristic condition can always be satisfied by choosing sufficiently large sub-characteristic speeds. However as we see in the next few paragraphs, the sub-characteristic speeds are the velocities $\{\pm a_p\}$ of the characteristic variables of the relaxation system. Larger $\{a_p\}$ imply a reduced CFL number and hence smaller time-steps, i.e. more computational effort. Also, large sub-characteristic speeds increase numerical diffusion. Hence it is desirable to choose the smallest $\{a_p\}$ that meet the stability criteria (Equation 15). For the Jin-Xin scheme, typically $\{a_p\}$ is set to λ, the maximum eigenvalue of the Jacobian $\mathbf{F}'(\mathbf{C})$.

The stiff source term introduced by the relaxation formulation can be handled by operator splitting, a simple and a popular technique used in advection-reaction and advection-diffusion problems (LeVeque 2002, Hundsdorfer and Verwer 2003, Younis and Gerritsen 2006). The relaxation system is split into two sub-problems, a homogenous advective system and an ODE system, that can be solved independently.

$$\begin{bmatrix}\mathbf{C}\\ \mathbf{V}\end{bmatrix}_{\mathbf{t}} + \begin{bmatrix}\mathbf{0} & \mathbf{I}\\ \mathbf{A}^2 & \mathbf{0}\end{bmatrix}\begin{bmatrix}\mathbf{C}\\ \mathbf{V}\end{bmatrix}_{\mathbf{x}} = \begin{bmatrix}0\\ 0\end{bmatrix}, \qquad \begin{bmatrix}\mathbf{C}\\ \mathbf{V}\end{bmatrix}_{\mathbf{t}} = \begin{bmatrix}0\\ 1/\varepsilon(\mathbf{F}(\mathbf{C})-\mathbf{V})\end{bmatrix}. \tag{16}$$

Homogenous advective system Stiff system of ODEs

This technique allows the use of high resolution methods for the advective system and standard ODE solvers for the stiff system of ODEs. Though Jin and Xin (1995) solve the stiff ODE system with an implicit RK method, the ODE part in our case can in fact be solved exactly. Using an explicit method would have resulted in very small time steps, dependent on ε. With implicit methods, it would have been necessary to solve a large system of algebraic equations. With operator splitting we avoid both pitfalls. Splitting does introduce an error, and since the source is stiff, naively using either a Godunov or a Strang splitting with a higher order time-stepping introduces an $O(\Delta t)$ error. A splitting scheme introduced by Jin (1995) ensures the error to be of order $O(\Delta t^r)$, by interspersing splitting steps with the time-steps of an *r*-stage RK scheme.

The homogenous advective part of the split relaxation system (Equation 16) has the form

$$\begin{bmatrix}\mathbf{C}\\ \mathbf{V}\end{bmatrix}_{\mathbf{t}} + \mathbf{B}\begin{bmatrix}\mathbf{C}\\ \mathbf{V}\end{bmatrix}_{\mathbf{x}} = \begin{bmatrix}\mathbf{0}\\ \mathbf{0}\end{bmatrix}, \quad \text{where } \mathbf{B} = \begin{bmatrix}\mathbf{0} & \mathbf{I}\\ \mathbf{A}^2 & \mathbf{0}\end{bmatrix}. \tag{17}$$

The matrix $\mathbf{B}$ has eigenvalues $\{\pm a_p\}$ and eigenvectors of the form $[1,0,0\ldots,a_p,0..0]^T$ and $[1,0,0\ldots,-a_p,0..0]^T$. For example, for the scalar conservation law the matrix **B**, the eigenvalues and the right eigenmatrix are given by

$$\mathbf{B} = \begin{bmatrix}0 & 1\\ a^2 & 0\end{bmatrix}, \ \mathbf{\Lambda} = \begin{bmatrix}a & 0\\ 0 & -a\end{bmatrix}, \ \mathbf{R} = \begin{bmatrix}1 & 1\\ a & -a\end{bmatrix} \quad \text{where } \mathbf{B} = \mathbf{R}\,\mathbf{\Lambda}\,\mathbf{R}^{-1}.$$

The spatial discretizations in the jth grid cell, for the homogenous system, with a uniform grid spacing $\Delta x = \Delta x_j = (x_{j+\frac{1}{2}} - x_{j-\frac{1}{2}})$, can be written as

$$\frac{\partial \mathbf{C}_j}{\partial t} + \frac{(\mathbf{V}_{j+\frac{1}{2}} - \mathbf{V}_{j-\frac{1}{2}})}{\Delta x_j} = 0, \tag{18a}$$

$$\frac{\partial \mathbf{V}_j}{\partial t} + \mathbf{A}^2\frac{(\mathbf{C}_{j+\frac{1}{2}} - \mathbf{C}_{j-\frac{1}{2}})}{\Delta x_j} = 0. \tag{18b}$$

To get the point values $\mathbf{C}_{j+\frac{1}{2}}$, $\mathbf{V}_{j+\frac{1}{2}}$, whose upwind direction cannot be determined directly, we use a characteristic decomposition on the constant relaxation matrix $\mathbf{B}$. The advective system can be diagonalized as

$$\mathbf{R}^{-1}\begin{bmatrix}\mathbf{C}\\ \mathbf{V}\end{bmatrix}_{\mathbf{t}} + \mathbf{R}^{-1}\mathbf{B}\begin{bmatrix}\mathbf{C}\\ \mathbf{V}\end{bmatrix}_{\mathbf{x}} = \begin{bmatrix}0\\ 0\end{bmatrix}, \tag{19}$$

$$\mathbf{W}_{\mathbf{t}} + \mathbf{\Lambda}\,\mathbf{W}_{\mathbf{x}} = \mathbf{0}.$$

The vector $\mathbf{W}$ is made up of the characteristic variables $\left\{W_p^{\pm} = V_p \pm a_p C_p\right\}$ that travel with speeds $\left\{\pm a_p\right\}$ respectively. While the original system has waves moving only from left to right, in the relaxation system, information flows in both directions. The characteristic variables $\left\{W_p^{\pm} = V_p \pm a_p C_p\right\}$ can be solved by upwind schemes to obtain $\mathbf{C}_{j+\frac{1}{2}}$ and $\mathbf{V}_{j+\frac{1}{2}}$. For example, with a first order upwind scheme the point values $\mathbf{C}_{j+\frac{1}{2}}$, $\mathbf{V}_{j+\frac{1}{2}}$ are obtained by

$$\left(\mathbf{V}+\mathbf{AC}\right)_{j+1/2} = \left(\mathbf{V}+\mathbf{AC}\right)_j, \qquad \left(\mathbf{V}-\mathbf{AC}\right)_{j+1/2} = \left(\mathbf{V}-\mathbf{AC}\right)_{j+1}, \tag{20}$$

$$\mathbf{C}_{j+1/2} = \frac{1}{2}\left(\mathbf{C}_j + \mathbf{C}_{j+1}\right) - \frac{1}{2}\mathbf{A}^{-1}\left(\mathbf{V}_{j+1} - \mathbf{V}_j\right), \tag{21a}$$

$$\mathbf{V}_{j+1/2} = \frac{1}{2}\left(\mathbf{V}_j + \mathbf{V}_{j+1}\right) - \frac{1}{2}\mathbf{A}\left(\mathbf{C}_{j+1} - \mathbf{C}_j\right). \tag{21b}$$

Using Equation (21), the first order semi-discrete approximation can be written as

$$\frac{\partial \mathbf{C}_j}{\partial t} + \frac{1}{2\Delta x_j}\left(\mathbf{V}_{j+1} - \mathbf{V}_{j-1}\right) - \frac{1}{2\Delta x_j}\mathbf{A}\left(\mathbf{C}_{j+1} - 2\mathbf{C}_j + \mathbf{C}_{j-1}\right) = 0, \tag{22a}$$

$$\frac{\partial \mathbf{V}_j}{\partial t} + \frac{1}{2\Delta x_j}\mathbf{A}^2\left(\mathbf{C}_{j+1} - \mathbf{C}_{j-1}\right) - \frac{1}{2\Delta x_j}\mathbf{A}\left(\mathbf{V}_{j+1} - 2\mathbf{V}_j + \mathbf{V}_{j-1}\right) = 0. \tag{22b}$$

Using forward Euler for time integration Equation (22a) is similar to the Lax-Friedrichs scheme. If we choose the sub-characteristic speeds $\left\{a_p = a\right\}$ such that $a\left(\Delta t/\Delta x\right) = 1$, this scheme collapses to the Lax-Friedrichs scheme.

The algorithm for the first order scheme is given by the following steps

1. Obtain $\begin{bmatrix}\mathbf{C}^* \\ \mathbf{V}^*\end{bmatrix}$ by solving analytically the ODE system $\begin{bmatrix}\mathbf{C}^n \\ \mathbf{V}^n\end{bmatrix}_t = \begin{bmatrix}0 \\ \frac{1}{\varepsilon}(\mathbf{F}(\mathbf{C}^n) - \mathbf{V}^n)\end{bmatrix}$,
2. Solve the homogenous advective system

$$\mathbf{C}^{n+1} = \mathbf{C}^* - \frac{\Delta t}{\Delta x_j}\left(\mathbf{V}^*_{j+\frac{1}{2}} - \mathbf{V}^*_{j-\frac{1}{2}}\right),$$

$$\mathbf{V}^{n+1} = \mathbf{V}^* - \frac{\Delta t}{\Delta x_j}\mathbf{A}^2\left(\mathbf{C}^*_{j+\frac{1}{2}} - \mathbf{C}^*_{j-\frac{1}{2}}\right),$$

using $\mathbf{V}^*_{j+\frac{1}{2}}$ and $\mathbf{C}^*_{j+\frac{1}{2}}$ as given in (21).

Jin and Xin present a second order scheme by using Van-Leer's MUSCL (Van Leer 1979) scheme for the spatial discretization and a RK-2 time stepping. Instead of using a piecewise constant reconstruction as in the first order method, the MUSCL scheme uses a piecewise linear function. An adaptive limiter controls the linear function used based on the upwind direction. Here the characteristic variables are updated as

$$\left(\mathbf{V}_p + a_p\mathbf{C}_p\right)_{j+1/2} = \left(\mathbf{V}_p + a_p\mathbf{C}_p\right)_j + \frac{1}{2}\Delta x_j \sigma_j^+ \tag{23}$$

$$\left(\mathbf{V}_p - a_p\mathbf{C}_p\right)_{j+1/2} = \left(\mathbf{V}_p - a_p\mathbf{C}_p\right)_{j+1} - \frac{1}{2}\Delta x_{j+1}\sigma^-_{j+1} \ ,$$

where

$$\sigma_j^{\pm} = \frac{1}{\Delta x_j}\left(\left(\mathbf{V}_p \pm a_p\mathbf{C}_p\right)_{j+1} - \left(\mathbf{V}_p \pm a_p\mathbf{C}_p\right)_j\right)\phi(\theta_j^{\pm}) \ . \tag{24a}$$

Here $\phi(\theta)$ is the limiter. A popular choice is the van Leer limiter $\phi(\theta) = \frac{|\theta| + \theta}{|\theta| + 1}$. θ is a measure of smoothness given by

$$\theta_j^{\pm} = \frac{\left(\mathbf{V}_p \pm a_p\mathbf{C}_p\right)_j - \left(\mathbf{V}_p \pm a_p\mathbf{C}_p\right)_{j-1}}{\left(\mathbf{V}_p \pm a_p\mathbf{C}_p\right)_{j+1} - \left(\mathbf{V}_p \pm a_p\mathbf{C}_p\right)_j} \ . \tag{24b}$$

Some other common high-resolution limiters are the minmod and superbee limiters (LeVeque 2002). The minmod limiter is known to be diffusive and will lead to smeared shocks. The superbee limiter resolves the shocks with little smearing but also tends to steepen and square off smooth variations. The van Leer limiter which resolves shocks well, but does not artificially steepen the smooth slopes is usually is a good choice for a wide class of problems, including ours.

Using the above, the algorithm for the second order scheme, with Jin's splitting, can be formulated as

1. First RK- Stage: Obtain $\begin{bmatrix}\mathbf{C}^* \\ \mathbf{V}^*\end{bmatrix}$ by solving analytically the ODE system $\begin{bmatrix}\mathbf{C}^n \\ \mathbf{V}^n\end{bmatrix}_t = \begin{bmatrix}0 \\ \frac{1}{\varepsilon}(\mathbf{F}(\mathbf{C}^n) - \mathbf{V}^n)\end{bmatrix}$,
2. First RK- Stage: Solve the homogenous advective system using the MUSCL scheme

$$\mathbf{C}^1 = \mathbf{C}^* - \frac{\Delta t}{\Delta x_j}\left(\mathbf{V}^*_{j+\frac{1}{2}} - \mathbf{V}^*_{j-\frac{1}{2}}\right),$$

$$\mathbf{V}^1 = \mathbf{V}^* - \frac{\Delta t}{\Delta x_j}\mathbf{A}^2\left(\mathbf{C}^*_{j+\frac{1}{2}} - \mathbf{C}^*_{j-\frac{1}{2}}\right),$$

   where $\mathbf{V}^*_{j+\frac{1}{2}}$ and $\mathbf{C}^*_{j+\frac{1}{2}}$ are obtained using given in (23) and (24),

3. Second RK- Stage: Obtain $\begin{bmatrix}\mathbf{C}^{**} \\ \mathbf{V}^{**}\end{bmatrix}$ by solving the ODE system $\begin{bmatrix}\mathbf{C}^1 \\ \mathbf{V}^1\end{bmatrix}_t = \begin{bmatrix}0 \\ \frac{1}{\varepsilon}(\mathbf{F}(\mathbf{C}^1) - \mathbf{V}^1)\end{bmatrix}$,
4. Second RK- Stage: Solve the homogenous advective system

$$\mathbf{C}^2 = \mathbf{C}^{**} - \frac{\Delta t}{\Delta x_j}\left(\mathbf{V}^{**}_{j+\frac{1}{2}} - \mathbf{V}^{**}_{j-\frac{1}{2}}\right),$$

$$\mathbf{V}^2 = \mathbf{V}^{**} - \frac{\Delta t}{\Delta x_j}\mathbf{A}^2\left(\mathbf{C}^{**}_{j+\frac{1}{2}} - \mathbf{C}^{**}_{j-\frac{1}{2}}\right),$$

where $\mathbf{V}^{**}_{j+\frac{1}{2}}$ and $\mathbf{C}^{**}_{j+\frac{1}{2}}$ are obtained using given in (23) and (24),

5. Take the RK-average

$$\begin{bmatrix}\mathbf{C}^{n+1}\\ \mathbf{V}^{n+1}\end{bmatrix} = \frac{1}{2}\begin{bmatrix}(\mathbf{C}^n + \mathbf{C}^2)\\ (\mathbf{V}^n + \mathbf{V}^2)\end{bmatrix}.$$

The modified equation (27) for the relaxation scheme indicates that the numerical diffusion can be reduced if the sub-characteristic speed a is varied to closely track $f'(u)$. There are two possible ways to construct a relaxation system with varying sub-characteristic. One is derived using a non-conservative form of the equations, the other using a conservative formulation, written as

Non-conservative form

$$\frac{\partial \mathbf{C}}{\partial t} + \frac{\partial \mathbf{V}}{\partial x} = 0,$$

$$\frac{\partial \mathbf{V}}{\partial t} + \mathbf{A}(x,t)^2\frac{\partial \mathbf{C}}{\partial x} = \frac{1}{\varepsilon}(\mathbf{F}(\mathbf{C}) - \mathbf{V}),$$

Conservative form

$$\frac{\partial \mathbf{C}}{\partial t} + \frac{\partial \mathbf{V}}{\partial x} = 0,$$

$$\frac{\partial \mathbf{V}}{\partial t} + \frac{\partial}{\partial x}\left(\mathbf{A}(x,t)^2\mathbf{C}\right) = \frac{1}{\varepsilon}(\mathbf{F}(\mathbf{C}) - \mathbf{V}),$$

written compactly as,

$$\mathbf{q}_t + \mathbf{B}(x,t)\mathbf{q}_x = \mathbf{s} \quad ,$$

or

$$\mathbf{q}_t + (\mathbf{B}(x,t)\mathbf{q})_x = \mathbf{s},$$

where $\mathbf{q} = \begin{bmatrix}\mathbf{C}\\ \mathbf{V}\end{bmatrix}$ and $\mathbf{B} = \begin{bmatrix}\mathbf{0} & \mathbf{I}\\ \mathbf{A}^2 & \mathbf{0}\end{bmatrix}$ as before.

For simplicity we use the non-conservative form. Of course, we can go back and forth between the forms at the expense of adding source terms. Since we have a stiff source term and we use operator splitting, using either form does not affect our numerical calculations.

Analysis of the variable relaxation scheme

Using a Chapman-Enskog expansion to represent $\mathbf{V}$, the first order approximation to the variable relaxation system becomes

$$\frac{\partial \mathbf{C}}{\partial t} + \frac{\partial \mathbf{F}(\mathbf{C})}{\partial x} = \varepsilon \frac{\partial}{\partial x}\left((\mathbf{A}(x,t)^2 - \mathbf{F}'(\mathbf{C})^2) \frac{\partial \mathbf{C}}{\partial x} \right) + \mathrm{O}(\varepsilon^2). \tag{28}$$

Again the term $\varepsilon(\mathbf{A}(x,t)^2 - \mathbf{F}'(\mathbf{C})^2)$ plays the role of diffusion coefficient matrix. Equation (28) is well-posed only if $(\mathbf{A}(x,t)^2 - \mathbf{F}'(\mathbf{C})^2)$ is positive semi-definite for all $\mathbf{C}$; this defines the sub-characteristic condition for the variable relaxation system. In 1D, this requirement reduces to

$$\lambda(x,t)^2 \le a(x,t)^2, \tag{29}$$

where $\lambda(x,t) = \max_{1 \le p \le n_c - 1} \left| \lambda_p(x,t) \right|$, $\quad a(x,t) = \min_{1 \le p \le n_c - 1} a_p(x,t)$,

and $\lambda_p(x,t)$ are the local eigenvalues of the Jacobian $\mathbf{F}'(\mathbf{C})$.

The local eigenvalues of the Jacobian $\mathbf{F}'(\mathbf{C})$ represent either the rarefaction speeds or the shock speeds. The sub-characteristic speeds must be chosen so that the positive semi-definiteness of the diffusion coefficient matrix is guaranteed in either case (Liu 1987). In the Jin-Xin relaxation this was done by setting the sub-characteristic speed $a = \max_{1 \le p \le n_c - 1} \left| \lambda_p(x,t) \right|, \forall (x,t)$. For the gas displacement example, the tie-line eigenvalue is given by $\frac{\partial F_1}{\partial C_1}$ (Equation 10a). The nontie-line eigenvalues hover around 1 and an estimate of the maximum nontie-line eigenvalue can be obtained (Dindoruk 1982). The sub-characteristic speeds are then chosen as

$$a_p(x,t) \ge \max\{ \frac{\partial F_1}{\partial C_1}(x,t), \frac{F_1(x+\frac{\Delta x}{2},t) - F_1(x-\frac{\Delta x}{2},t)}{C_1(x+\frac{\Delta x}{2},t) - C_1(x-\frac{\Delta x}{2},t)}, \max_{(x,t)} \lambda_{\mathrm{NTL}}(x,t) \}. \tag{30}$$

Numerical solution

Like before, we use operator splitting where the relaxation system is split into two sub-problems, a homogenous advective system and an ODE system. The only difference here lies in the way the homogenous system is solved.

In the Jin-Xin relaxation system the matrix $\mathbf{B}$ is diagonalizable and the values of C_p and V_p at the interfaces $\{x_{j+1/2}\}$ are obtained by using the characteristic variables $\{\mathrm{W}_p^{\pm} = \mathrm{V}_p \pm a_p \mathrm{C}_p\}$. With the variable system, we cannot diagonalize the homogenous system as easily as before. The

eigenmatrix $\mathbf{R}$ of this system depends on its eigenvalues. When the eigenvalues are variable in *(x,t)* the eigenmatrix also becomes variable in (x,t), and $\mathbf{B}(x,t) = \mathbf{R}(x,t)\mathbf{\Lambda}(x,t)\mathbf{R}^{-1}(x,t)$. For example, for the 2-component displacement (the scalar conservation law), we have

$$\mathbf{B}(x,t) = \begin{bmatrix} 0 & 1 \\ a(x,t)^2 & 0 \end{bmatrix}, \quad \mathbf{\Lambda}(x,t) = \begin{bmatrix} a(x,t) & 0 \\ 0 & -a(x,t) \end{bmatrix}, \quad \mathbf{R}(\mathrm{x},\mathrm{t}) = \begin{bmatrix} 1 & -1 \\ a(x,t) & a(x,t) \end{bmatrix}.$$

Multiplying the homogeneous advection system $\mathbf{q}_t + \mathbf{B}(x,t)\mathbf{q}_x = 0$ with $\mathbf{R}^{-1}$, we get

$$\mathbf{R}^{-1}(x,t)\mathbf{q}_t + \mathbf{R}^{-1}(x,t)\mathbf{B}(x,t)\mathbf{q}_x = \mathbf{0}.$$

This can be written as

$$\mathbf{w}_t + \mathbf{\Lambda}(x,t)\,\mathbf{w}_x = \left(\mathbf{R}_t^{-1}(x,t) + \mathbf{\Lambda}(x,t)\mathbf{R}_x^{-1}(x,t)\right)\mathbf{R}(x,t)\,\mathbf{w}, \text{ where } \mathbf{w} = \mathbf{R}^{-1}(x,t)\mathbf{q},$$

because $\mathbf{R}^{-1}(x,t)\mathbf{q}_t = (\mathbf{R}^{-1}(x,t)\mathbf{q})_t - \mathbf{R}_t^{-1}(x,t)\mathbf{q}$ and $\mathbf{R}^{-1}(x,t)\mathbf{q}_x = (\mathbf{R}^{-1}(x,t)\mathbf{q})_x - \mathbf{R}_x^{-1}(x,t)\mathbf{q}$.

The advection equations are now coupled together by the source terms, and the left and the right going waves do not propagate independently. Rather than working with this system, we rather view the system as a set of Riemann problems at the interfaces $\{x_{j+1/2}\}$ (LeVeque 2002) that can be easily solved numerically.

Define $\mathbf{q}_j^n = \left[\mathbf{C}_j^n \;\; \mathbf{V}_j^n\right]^{\mathrm{T}} = \left[C_{1,j}^n \;,\; C_{2,j}^n \;\; \ldots \;\; C_{n_c-1,j}^n, \;\; V_{1,j}^n \;,\; V_{2,j}^n \;\; \ldots \;\; V_{n_c-1,j}^n\right]^{\mathrm{T}}$, $\Delta\mathbf{q}_{j\text{-}\frac{1}{2}}^n = \mathbf{q}_j^n - \mathbf{q}_{j\text{-}1}^n$.
Also, define the right eigenmatrix $\mathbf{R}_{\mathrm{j}\text{-}\frac{1}{2}} = [\mathbf{r}_{\mathrm{j}\text{-}\frac{1}{2}}^1 \;\; \mathbf{r}_{\mathrm{j}\text{-}\frac{1}{2}}^2 \;\; \ldots \;\; \mathbf{r}_{\mathrm{j}\text{-}\frac{1}{2}}^{2(\mathrm{n_c}\text{-}1)}]$ and the left eigenmatrix $\mathbf{L}_{j\text{-}\frac{1}{2}} = [\left(\ell_{j\text{-}\frac{1}{2}}^1\right)^{\mathrm{T}} \;\; \left(\ell_{j\text{-}\frac{1}{2}}^2\right)^{\mathrm{T}} \ldots \left(\ell_{j\text{-}\frac{1}{2}}^{2(\mathrm{n_c}\text{-}1)}\right)^{\mathrm{T}}]$.

Set $\mathbf{\Lambda}_{j\text{-}\frac{1}{2}}^+$ and $\mathbf{\Lambda}_{j\text{-}\frac{1}{2}}^-$ such that $\mathbf{B}_{j\text{-}\frac{1}{2}} = \mathbf{R}_{j\text{-}\frac{1}{2}}\,\mathbf{\Lambda}_{j\text{-}\frac{1}{2}}\mathbf{L}_{j\text{-}\frac{1}{2}} = \mathbf{R}_{j\text{-}\frac{1}{2}}\left(\mathbf{\Lambda}_{j\text{-}\frac{1}{2}}^+ + \mathbf{\Lambda}_{j\text{-}\frac{1}{2}}^-\right)\mathbf{L}_{j\text{-}\frac{1}{2}}$,
$\mathbf{B}_{j\text{-}\frac{1}{2}}^+ = \mathbf{R}_{j\text{-}\frac{1}{2}}\mathbf{\Lambda}_{j\text{-}\frac{1}{2}}^+\mathbf{L}_{j\text{-}\frac{1}{2}}$, and $\mathbf{B}_{j\text{-}\frac{1}{2}}^- = \mathbf{R}_{j\text{-}\frac{1}{2}}\mathbf{\Lambda}_{j\text{-}\frac{1}{2}}^-\mathbf{L}_{j\text{-}\frac{1}{2}}$, where $\mathbf{\Lambda}_{j\text{-}\frac{1}{2}}^+ = diag\left(\lambda_1^+, \lambda_2^+ \cdots \lambda_{2(\mathrm{n_c}-1)}^+\right)$ with $\lambda_k^+ = \max(\lambda_k, 0)$, and $\mathbf{\Lambda}_{j\text{-}\frac{1}{2}}^- = diag\left(\lambda_1^-, \lambda_2^- \cdots \lambda_{2(\mathrm{n_c}-1)}^-\right)$ with $\lambda_k^- = \min(\lambda_k, 0)$.

We write the update at every time step as

$$\mathcal{D}_+\mathbf{q}_j^n = \frac{1}{\Delta x}(\mathbf{q}_{j+\frac{1}{2}}^n - \mathbf{q}_{j-\frac{1}{2}}^n) \;=\; \frac{1}{\Delta x}(\mathbf{B}_{j\text{-}\frac{1}{2}}^+\Delta\mathbf{q}_{j\text{-}\frac{1}{2}}^n + \mathbf{B}_{j+\frac{1}{2}}^-\Delta\mathbf{q}_{j+\frac{1}{2}}^n). \tag{31}$$

The first order variable relaxation method can now be constructed as

1. Choose $a_p(x_j, t_n)$ as given in Equation (30) so as to satisfy the sub-characteristic condition,

2. Obtain $\begin{bmatrix} \mathbf{C}^* \\ \mathbf{V}^* \end{bmatrix}$ by solving analytically the ODE system $\begin{bmatrix} \mathbf{C}^n \\ \mathbf{V}^n \end{bmatrix}_t = \begin{bmatrix} 0 \\ \frac{1}{\varepsilon}(\mathbf{F}(\mathbf{C}^n) - \mathbf{V}^n) \end{bmatrix}$ as

$$\mathbf{C}_j^* = \mathbf{C}_j^n$$

$$\mathbf{V}_j^* = F(\mathbf{C}_j^*)\left(1 - e^{-\Delta t/\varepsilon}\right) + \mathbf{V}_j^n e^{-\Delta t/\varepsilon}, \quad \mathbf{q}_j^* = \begin{bmatrix} \mathbf{C}_j^* \\ \mathbf{V}_j^* \end{bmatrix}$$

3. Solve the homogenous advective system
$\mathbf{q}_j^{n+1} = \mathbf{q}_j^* - \Delta t\, \mathcal{D}_+ \mathbf{q}_j^*$ where $\mathcal{D}_+ \mathbf{q}_j^*$ is the update as given in Equation (31).

If implemented in matrix form, as given above, the method can be computationally expensive. But the right and left eigenvectors have a simple analytical form, which can be exploited to arrive at updates to individual components, in a manner similar to Jin-Xin updates. The right eigenvectors corresponding to the pth component have the form,

$$\mathbf{r}_{j-\frac{1}{2}}^k = [0 \ldots \underset{\substack{\uparrow \\ p^{\text{th}}\text{ element}}}{1}\ 0 \cdots 0\ \underset{\substack{\uparrow \\ (n_c+p-1)^{\text{th}}\text{ element}}}{a_{p,j}}\ 0 \cdots 0]^{\mathrm{T}}, \qquad \mathbf{r}_{j-\frac{1}{2}}^{k+1} = [0 \ldots \underset{\substack{\uparrow \\ p^{\text{th}}\text{ element}}}{1}\ 0 \cdots 0\ \underset{\substack{\uparrow \\ (n_c+p-1)^{\text{th}}\text{ element}}}{-a_{p,j-1}}\ 0 \cdots 0]^{\mathrm{T}},$$

and the left eigenvectors corresponding to the pth component are of the form

$$\ell_{j-\frac{1}{2}}^k = \left[0 \ldots \underset{\substack{\uparrow \\ p^{\text{th}}\text{ element}}}{\frac{a_{p,j-1}}{a_{p,j} + a_{p,j-1}}}\ 0 \cdots 0\ \underset{\substack{\uparrow \\ (n_c+p-1)^{\text{th}}\text{ element}}}{\frac{1}{a_{p,j} + a_{p,j-1}}}\ 0 \cdots 0\right],$$

$$\ell_{j-\frac{1}{2}}^{k+1} = \left[0 \ldots \underset{\substack{\uparrow \\ p^{\text{th}}\text{ element}}}{\frac{a_{p,j}}{a_{p,j} + a_{p,j-1}}}\ 0 \cdots 0\ \underset{\substack{\uparrow \\ (n_c+p-1)^{\text{th}}\text{ element}}}{\frac{-1}{a_{p,j} + a_{p,j-1}}}\ 0 \cdots 0\right].$$

Here k is related to p as $k = 2p - 1$. Using this information, the update for the pth component of $\mathbf{C}$ and $\mathbf{V}$, in the 3rd step will be

$$C_{p,j}^{n+1} = C_{p,j}^n - \frac{\Delta t}{\Delta x}\left(\frac{a_{p,j} a_{p,j-1}}{a_{p,j} + a_{p,j-1}}\left(C_{p,j}^n - C_{p,j-1}^n\right) + \frac{-a_{p,j+1} a_{p,j}}{a_{p,j+1} + a_{p,j}}\left(C_{p,j+1}^n - C_{p,j}^n\right) \right)$$
$$- \frac{\Delta t}{\Delta x}\left(\frac{a_{p,j}}{a_{p,j} + a_{p,j-1}}\left(V_{p,j}^n - V_{p,j-1}^n\right) + \frac{a_{p,j}}{a_{p,j+1} + a_{p,j}}\left(V_{p,j+1}^n - V_{p,j}^n\right) \right),$$

$$V_{p,j}^{n+1} = V_{p,j}^{n} - \frac{\Delta t}{\Delta x}\left(\frac{(a_{p,j})^2 a_{p,j-1}}{a_{p,j}+a_{p,j-1}}\left(C_{p,j}^{n} - C_{p,j-1}^{n}\right) + \frac{a_{p,j+1}(a_{p,j})^2}{a_{p,j+1}+a_{p,j}}\left(C_{p,j+1}^{n} - C_{p,j}^{n}\right)\right)$$
$$- \frac{\Delta t}{\Delta x}\left(\frac{(a_{p,j})^2}{a_{p,j}+a_{p,j-1}}\left(V_{p,i}^{n} - V_{p,i-1}^{n}\right) - \frac{(a_{p,j})^2}{a_{p,j+1}+a_{p,j}}\left(V_{p,j+1}^{n} - V_{p,j}^{n}\right)\right).$$

High resolution variable relaxation

A second order high resolution method can be obtained by extending the first order method with appropriate wave limiters as before. But, in this case, the limiters, which depend on the characteristic variables and the magnitude of change in the characteristic waves, must be constructed using the left and right eigenvectors as follows

- Find the change in each of the *2(n$_c$-1)* characteristic variables using the corresponding left eigenvectors as $\alpha_{j-\frac{1}{2}}^{k} = \ell_{j-\frac{1}{2}}^{k} \bullet \Delta\mathbf{q}_{j-\frac{1}{2}}^{n}$ and the jump in the characteristic waves as $\mathbf{w}_{j-\frac{1}{2}}^{k} = \alpha_{j-\frac{1}{2}}^{k}\mathbf{r}_{j-\frac{1}{2}}^{k}$.
- Set the smoothness parameters of van Leer limiter equal to $\theta_{k,j-\frac{1}{2}} = \dfrac{\mathbf{w}_{I-\frac{1}{2}}^{k} \bullet \mathbf{w}_{j-\frac{1}{2}}^{k}}{\mathbf{w}_{j-\frac{1}{2}}^{k} \bullet \mathbf{w}_{j-\frac{1}{2}}^{k}}$, where $I = j-1$ for waves moving right (k odd) and $I = j+1$ for waves moving left (k even).
- Compute the second order updates as

$$\mathbf{q}_{j}^{n+1} = \mathbf{q}_{j}^{n} - \frac{\Delta t}{\Delta x}\left(\mathbf{B}_{j-\frac{1}{2}}^{+}\Delta\mathbf{q}_{j-\frac{1}{2}}^{n} + \mathbf{B}_{j+\frac{1}{2}}^{-}\Delta\mathbf{q}_{j+\frac{1}{2}}^{n}\right) - \frac{\Delta t}{\Delta x}\left(\mathcal{F}_{j+\frac{1}{2}}^{h} - \mathcal{F}_{j-\frac{1}{2}}^{h}\right),$$

where the higher order correction terms $\mathcal{F}_{j-\frac{1}{2}}^{h}$ are given by

$$\mathcal{F}_{j-\frac{1}{2}}^{h} = \frac{1}{2}\sum_{p=1,2\ldots} a_{p,j}\phi\left(\theta_{k,j-\frac{1}{2}}\right)\mathbf{w}_{j-\frac{1}{2}}^{k} + a_{p,j-1}\phi\left(\theta_{k+1,j-\frac{1}{2}}\right)\mathbf{w}_{j-\frac{1}{2}}^{k+1}, \quad \text{with } k = 2p-1.$$

We now define the update operator

$$\mathcal{D}_{+}\mathbf{q}_{j}^{n} = \frac{1}{\Delta x}(\mathbf{B}_{j-\frac{1}{2}}^{+}\Delta\mathbf{q}_{j-\frac{1}{2}}^{n} + \mathbf{B}_{j+\frac{1}{2}}^{-}\Delta\mathbf{q}_{j+\frac{1}{2}}^{n}) + \frac{1}{\Delta x}(\mathcal{F}_{j+\frac{1}{2}}^{h} - \mathcal{F}_{j-\frac{1}{2}}^{h}) \tag{35}$$

With this, the second order variable relaxation scheme can be given by the following algorithm

1. Choose $a_p(x_j, t_n)$ as given in Equation (30) so as to satisfy the sub-characteristic condition

2. First RK- Stage: Obtain $\begin{bmatrix} \mathbf{C}^* \\ \mathbf{V}^* \end{bmatrix}$ by solving analytically the ODE system $\begin{bmatrix} \mathbf{C}^n \\ \mathbf{V}^n \end{bmatrix}_t = \begin{bmatrix} 0 \\ \frac{1}{\varepsilon}(\mathbf{F}(\mathbf{C}^n) - \mathbf{V}^n) \end{bmatrix}$ as

$$\mathbf{C}_j^* = \mathbf{C}_j^n$$

$$\mathbf{V}_j^* = F(\mathbf{C}_j^*)\left(1 - e^{-\Delta t/\varepsilon}\right) + \mathbf{V}_j^n e^{-\Delta t/\varepsilon}, \quad \mathbf{q}_j^* = \begin{bmatrix} \mathbf{C}_j^* \\ \mathbf{V}_j^* \end{bmatrix}$$

3. First RK- Stage: Solve the homogenous advective system using the update operator given in Equation (35)

$$\mathbf{q}_j^{(1)} = \mathbf{q}_j^* - \Delta t\, \mathcal{D}_+ \mathbf{q}_j^*, \quad \mathbf{q}_j^{(1)} = \begin{bmatrix} \mathbf{C}_j^{(1)} \\ \mathbf{V}_j^{(1)} \end{bmatrix}$$

4. Second RK-Stage: Obtain $\begin{bmatrix} \mathbf{C}^{**} \\ \mathbf{V}^{**} \end{bmatrix}$ by solving the ODE system $\begin{bmatrix} \mathbf{C}^{(1)} \\ \mathbf{V}^{(1)} \end{bmatrix}_t = \begin{bmatrix} 0 \\ \frac{1}{\varepsilon}(\mathbf{F}(\mathbf{C}^{(1)}) - \mathbf{V}^{(1)}) \end{bmatrix}$ as

$$\mathbf{C}_j^{**} = \mathbf{C}_j^{(1)}$$

$$\mathbf{V}_j^{**} = F(\mathbf{C}_j^*)(1 - e^{-\Delta t/\varepsilon}) + \mathbf{V}_j^{(1)} e^{-\Delta t/\varepsilon}, \quad \mathbf{q}_j^{**} = \begin{bmatrix} \mathbf{C}_j^{**} \\ \mathbf{V}_j^{**} \end{bmatrix},$$

5. Second RK-Stage: Solve the homogenous advective system using the update operator given in Equation (35)

$$\mathbf{q}_j^{(2)} = \mathbf{q}_j^{**} - \Delta t\, \mathcal{D}_+ \mathbf{q}_j^{**}, \quad \mathbf{q}_j^{(2)} = \begin{bmatrix} \mathbf{C}_j^{(2)} \\ \mathbf{V}_j^{(2)} \end{bmatrix}$$

6. Take the RK-average

$$\mathbf{q}_j^{n+1} = \frac{1}{2}(\mathbf{q}_j^n + \mathbf{q}_j^{(2)}), \qquad \text{set } \mathbf{q}_j^{n+1} = \begin{bmatrix} \mathbf{C}_j^{n+1} \\ \mathbf{V}_j^{n+1} \end{bmatrix}$$

Again, the update of Equation (35) can be implemented in terms of individual components without matrix-vector operations as

$$C_{p,j}^{n+1} = C_{p,j}^{n} - \frac{\Delta t}{\Delta x}\left(\frac{a_{p,j}a_{p,j-1}}{a_{p,j}+a_{p,j-1}}\left(C_{p,j}^{n} - C_{p,j-1}^{n}\right) + \frac{-a_{p,j+1}a_{p,j}}{a_{p,j+1}+a_{p,j}}\left(C_{p,j+1}^{n} - C_{p,j}^{n}\right) \right)$$
$$- \frac{\Delta t}{\Delta x}\left(\frac{a_{p,j}}{a_{p,j}+a_{p,j-1}}\left(V_{p,j}^{n} - V_{p,j-1}^{n}\right) + \frac{a_{p,j}}{a_{p,j+1}+a_{p,j}}\left(V_{p,j+1}^{n} - V_{p,j}^{n}\right) \right) - \frac{\Delta t}{\Delta x}\left(C_{p,j+\frac{1}{2}}^{h} - C_{p,j-\frac{1}{2}}^{h}\right),$$

where the second order corrections $C_{p,j-\frac{1}{2}}^{h}$ are computed as

$$C_{p,j-\frac{1}{2}}^{h} = \frac{a_{p,j}}{2}\phi\left(\theta_{k,j-\frac{1}{2}}\right)\left(\frac{a_{p,j-1}}{a_{p,j}+a_{p,j-1}}\left(C_{p,j}^{n} - C_{p,j-1}^{n}\right) + \frac{1}{a_{p,j}+a_{p,j-1}}\left(V_{p,j}^{n} - V_{p,j-1}^{n}\right) \right) +$$
$$\frac{a_{p,j-1}}{2}\phi\left(\theta_{k+1,j-\frac{1}{2}}\right)\left(\frac{a_{p,j}}{a_{p,j}+a_{p,j-1}}\left(C_{p,j}^{n} - C_{p,j-1}^{n}\right) - \frac{1}{a_{p,j}+a_{p,j-1}}\left(V_{p,j}^{n} - V_{p,j-1}^{n}\right) \right).$$

The corresponding $V_{p,j}^{n+1}$ can be updated as

$$V_{p,j}^{n+1} = V_{p,j}^{n} - \frac{\Delta t}{\Delta x}\left(\frac{(a_{p,j})^2 a_{p,j-1}}{a_{p,j}+a_{p,j-1}}\left(C_{p,j}^{n} - C_{p,j-1}^{n}\right) + \frac{a_{p,j+1}(a_{p,j})^2}{a_{p,j+1}+a_{p,j}}\left(C_{p,j+1}^{n} - C_{p,j}^{n}\right) \right)$$
$$- \frac{\Delta t}{\Delta x}\left(\frac{(a_{p,j})^2}{a_{p,j}+a_{p,j-1}}\left(V_{p,j}^{n} - V_{p,j-1}^{n}\right) - \frac{(a_{p,j})^2}{a_{p,j+1}+a_{p,j}}\left(V_{p,j+1}^{n} - V_{p,j}^{n}\right) \right) - \frac{\Delta t}{\Delta x}\left(V_{p,j+\frac{1}{2}}^{h} - V_{p,j-\frac{1}{2}}^{h}\right),$$

where the second order corrections $V_{p,j-\frac{1}{2}}^{h}$ are computed as

$$V_{p,j-\frac{1}{2}}^{h} = \frac{a_{p,j}}{2}\phi\left(\theta_{k,j-\frac{1}{2}}\right)\left(\frac{a_{p,j}a_{p,j-1}}{a_{p,j}+a_{p,j-1}}\left(C_{p,j}^{n} - C_{p,j-1}^{n}\right) + \frac{a_{p,j}}{a_{p,j}+a_{p,j-1}}\left(V_{p,j}^{n} - V_{p,j-1}^{n}\right) \right) +$$
$$\frac{a_{p,j-1}}{2}\phi\left(\theta_{k+1,j-\frac{1}{2}}\right)\left(\frac{-a_{p,j}a_{p,j-1}}{a_{p,j}+a_{p,j-1}}\left(C_{p,j}^{n} - C_{p,j-1}^{n}\right) + \frac{a_{p,j-1}}{a_{p,j}+a_{p,j-1}}\left(V_{p,j}^{n} - V_{p,j-1}^{n}\right) \right).$$

The limiters are computed as

$$\theta_{k,j-\frac{1}{2}} = \frac{\left(\frac{a_{p,j-2}}{a_{p,j-1}+a_{p,j-2}}\left(C_{p,j-1}^{n} - C_{p,j-2}^{n}\right) + \frac{1}{a_{p,j-1}+a_{p,j-2}}\left(V_{p,j-1}^{n} - V_{p,j-2}^{n}\right) \right)\left(1 + a_{p,j}a_{p,j-1}\right)}{\left(\frac{a_{p,j-1}}{a_{p,j}+a_{p,j-1}}\left(C_{p,j}^{n} - C_{p,j-1}^{n}\right) + \frac{1}{a_{p,j}+a_{p,j-1}}\left(V_{p,j}^{n} - V_{p,j-1}^{n}\right) \right)\left(1 + a_{p,j}a_{p,j}\right)},$$

$$\theta_{k+1,j-\frac{1}{2}} = \frac{\left(\frac{a_{p,j+1}}{a_{p,j}+a_{p,j+1}}\left(C_{p,j+1}^{n} - C_{p,j}^{n}\right) - \frac{1}{a_{p,j}+a_{p,j+1}}\left(V_{p,j+1}^{n} - V_{p,j}^{n}\right) \right)\left(1 + a_{p,j-1}a_{p,j+1}\right)}{\left(\frac{a_{p,j}}{a_{p,j}+a_{p,j-1}}\left(C_{p,j}^{n} - C_{p,j-1}^{n}\right) - \frac{1}{a_{p,j}+a_{p,j-1}}\left(V_{p,j}^{n} - V_{p,j-1}^{n}\right) \right)\left(1 + a_{p,j-1}a_{p,j-1}\right)}.$$

3. Experimental

We have been unsuccessful so far in attracting a student or postdoctoral student to complete the experimental part of this project, despite interviewing several candidates over the last year.

4. Results and discussion

This report covers the second six months of the second year of our research grant. The six months were used primarily to investigate important numerical and computational issues related to compositional streamline simulation for gas injection processes: accurate simulation of the strongly nonlinear systems governing transport, and grid orientation effects.

4.1. Relaxation schemes

We have closed our investigation of 1D relaxation schemes, and have moved on to two spatial dimensions.

Tables 1 and 2 give the comparison of the results of the Jin's splitting and the Strang splitting with RK-2 scheme on the linear advection equation and Burgers equation with periodic initial data**.** For the linear advection equation, the Strang splitting behaves just as well as Jin splitting. But for the Burgers equation, the order of accuracy of the Strang splitting reduces to $O(\Delta t)$, while Jin's splitting maintains $O(\Delta t^2)$.

TABLE 1

L^1 and L^∞ - rate of convergence for the linear advection equation

$u_t + u_x = 0, \quad u(x,0) = \sin(x)$**,** CFL = 0.5

S-RK2: 2nd order relaxation scheme with Strang splitting,
J-RK2: 2nd order relaxation scheme with Jin's splitting,
TVD-RK2: 2nd order upwind TVD-RK2 scheme

	L^1 rate of convergence			L^∞ error convergence		
N	S-RK2	J-RK2	TVD-RK2	S-RK2	J-RK2	TVD-RK2
80	2.0155	2.0155	2.0155	1.4120	1.4120	1.4120
160	2.0159	2.0159	2.0159	1.3576	1.3576	1.3576
320	2.0299	2.0299	2.0299	1.3587	1.3587	1.3587
640	2.0277	2.0277	2.0272	1.3213	1.3213	1.3200

TABLE 2

L^1 and L^∞ - rate of convergence for Burgers equation (pre-shock solution)

$u_t + uu_x = 0, \quad u(x,0) = \sin(x)$**,** CFL = 0.5, T = 0.35

S-RK2: 2nd order relaxation scheme with Strang splitting,
J-RK2: 2nd order relaxation scheme with Jin's splitting,

TVD-RK2: 2nd order upwind TVD-RK2 scheme

	L^1 rate of convergence			L^∞ error convergence		
N	S-RK2	J-RK2	TVD-RK2	S-RK2	J-RK2	TVD-RK2
80	1.0624	1.9230	1.9227	0.7684	1.3972	0.9893
160	1.0162	2.0039	1.9689	0.9083	1.2919	0.9973
320	1.0143	2.0069	1.9787	0.9521	1.3357	0.9993
640	1.0095	2.0183	1.9918	0.9748	1.4094	0.9998

Figure 12 shows the result of first order relaxation schemes on the two-component displacement (Equation 8). Since this is a scalar system we have only two characteristic waves moving with sub-characteristic speeds $\pm a$. By the sub-characteristic condition (Equation 15) the magnitude of the sub-characteristic speed must be at least $\max f'(S)$.

The effect of increasing the sub-characteristic speed can also be seen in Figure 12. It is clear that as the sub-characteristic speed is increased the numerical diffusion increases. While SPU resolves the zero-speed trailing shock sharply for test case 2, the relaxation scheme smears this shock. These behaviors can be better understood by comparing the modified equations for SPU and the first-order relaxation scheme. We performed the analysis on a linear advective system for simplicity. The system is given by

$$u_t + f(u)_x = 0, \text{ with } f(u) = cu, \text{ where } c \text{ is a constant.}$$

The modified equation for SPU is given by

$$u_t + f(u)_x = \frac{1}{2}(f'\Delta x - \Delta t(f')^2)u_{xx} + O(\Delta x^2),$$

while the modified equation for the first order relaxation scheme is of the form

$$u_t + f(u)_x = \frac{1}{2}(a\Delta x - \Delta t(f')^2)u_{xx} + O(\Delta x^2).$$

The modified equations show that while the diffusion coefficient of SPU decreases as $f'(u)$ decreases, the diffusion coefficient of the relaxation scheme depends on the sub-characteristic speed a. It increases when a increases, and when $f'(u)$ decreases. When the speed $f'(u)$ tends to zero, the diffusion coefficient of SPU also tends to zero, but the diffusion coefficient of the relaxation scheme tends to $0.5(a\Delta x)$. The diffusion of the relaxation scheme also increases with the relaxation rate ε. However, as shown by Equation (14), this is of magnitude $O(\varepsilon)$ and since we always take ε very small, this is negligible.

For the ternary systems, the sub-characteristic speed must be decided based on the tieline and non-tieline eigenvalues (Equation 10). The sub-characteristic speeds must be at least $a_p = \max_x \{\lambda_{TL}(x), \lambda_{NTL}(x)\}$. As before, the first order relaxation scheme exhibits more diffusion than SPU. The higher order relaxation scheme has less diffusion and the solution profile (Figure 13b) shows that the results are very close to component-wise upwind TVD-RK2 scheme. However, in phase space (Figures 13a and 14) we see differences in the behavior of the upwind and relaxation schemes. For finer grids, at the equal eigenvalue point the relaxation scheme,

unlike the upwind TVD –RK2 scheme, stays close to the MOC path. Along the initial tieline however, the relaxation scheme exhibits slightly more non-physical diffusion. Our goal in the next section is to modify the relaxation scheme to reduce numerical diffusion while retaining strong hyperbolicity.

Figures 15a and 15b show the results of the first order variable relaxation scheme for the two-component displacements (Equation 8). The numerical diffusion of the first order variable relaxation scheme is reduced significantly when the variable sub-characteristic speed is very close to the eigenvalues of the original system. In particular in test case 2, the variable relaxation scheme resolves the zero-speed trailing shock with very little diffusion.

For the ternary systems, the solutions of the first order variable relaxation scheme are very close to those of SPU. The higher order variable relaxation (Figures 16a and 17) scheme has no nonphysical diffusion along the initial tie-line and stays close to the MOC path at the equal eigenvalue point in phase space. In fact, the results are very similar to those obtained with third order ENO-RK3. In general, we have observed that in many cases the second order variable relaxation scheme was competitive with third order component-wise ENO-RK3 reconstruction, and at least as good as the second order component-wise TVD-RK2 with van Leer limiting.

Would α–β relaxation help?

A more general form of the relaxation system can be formulated for the scalar conservation law as

$$\begin{bmatrix} u \\ v \end{bmatrix}_t + \begin{bmatrix} 0 & 1 \\ \alpha & \beta \end{bmatrix} \begin{bmatrix} u \\ v \end{bmatrix}_x = \begin{bmatrix} 0 \\ -\frac{1}{\varepsilon}\left(v - f(u)\right) \end{bmatrix} \tag{39}$$

where $\mathbf{B} = \begin{bmatrix} 0 & 1 \\ \alpha & \beta \end{bmatrix}$ is the coefficient matrix. (40)

Here, $\alpha = -\lambda_1\lambda_2$ and $\beta = \lambda_1 + \lambda_2$ with λ_1, λ_2 being the eigenvalues of the coefficient matrix $\mathbf{B}$.

If $\mathbf{B}$ is constant, we can diagonalize the system as before. The characteristic variables are now $v - \lambda_2 u$ and $v - \lambda_1 u$, moving with speeds λ_1 and λ_2 respectively. Note that, when $\lambda_1 = -\lambda_2 = a$, that is $\alpha = -\lambda_1\lambda_2 = a^2$ and $\beta = \lambda_1 + \lambda_2 = 0$, this system reduces to the Jin-Xin relaxation system and when $\lambda_1 = a$, $\lambda_2 = 0$, it reduces to the upwind scheme of the same order.

The $O(\varepsilon)$ diffusion term, that arises as a result of using the Chapman-Enskog expansion for v, is $\varepsilon\beta(u) = \varepsilon(\lambda_1 - f'(u))(f'(u) - \lambda_2)$. For a system with positive speeds, $0 \le f'(u) \le f'_{\max}$, the sub-characteristic condition requires $\lambda_2 \le 0$ and $\lambda_1 \ge f'_{\max}$. To be as close as possible to the physical flux and yet obey the sub-characteristic condition, we can set $\lambda_1 = f'_{max}$ and $\lambda_2 = -\tau$, where τ is a positive number. Based on the choice of λ_2, the performance of this new scheme is between Jin-Xin relaxation ($\tau = f'_{\max}$) and the upwind scheme ($\tau = 0$). Finding optimal negative

eigenvalues that minimize numerical diffusion and yet ensure that the scheme behaves well at the weak hyperbolic points like the Jin-Xin system, is problem dependent. Therefore, the constant version of the general $\alpha - \beta$ relaxation is impractical .

Would a variable $\alpha - \beta$ give improved results? Again looking at the variable $\alpha - \beta$ system for the scalar conservation law, we see that the Chapman-Enskog requires the sub-characteristic condition $\lambda_2 \le f'(u) \le \lambda_1$. One way to reduce numerical diffusion would be to vary both eigenvalues λ_1 and λ_2 such that they are close to the local speeds. For example, we could set $\lambda_1 = f'(u) + \mathrm{O}(\Delta x)$ and $\lambda_2 = f'(u) - \mathrm{O}(\Delta x)$. This method however fails because the eigenvectors of the relaxation system are $[1 \ \lambda_1]^{\mathrm{T}}$ and $[1 \ \lambda_2]^{\mathrm{T}}$, and with $\lambda_1 = f'(u) + \mathrm{O}(\Delta x)$ and $\lambda_2 = f'(u) - \mathrm{O}(\Delta x)$, the eigenvectors are almost parallel to each other, which re-introduces weak hyperbolicity in the system. A more promising way is to vary only λ_1 so that it is close to the local speeds and keep λ_2 constant and close to $-f'_{max}$. This version is competitive to the variable version of Jin-Xin scheme. Note that for small λ_2 however, we end up with a nearly singular relaxation matrix and the scheme behaves just like the corresponding upwind scheme**.**

5. Conclusions

Although we are happy with the results we have obtained so far, we are behind schedule. This delay is caused by the difficulties we've experienced in finding appropriate postdoctoral students in both the computational and experimental area. Fortunately, we managed to attract Dr. Henrik Loef who started his postdoc with us November 1, 2006 on the no-cost extension we received for this project. As you are aware, funding for this project was cut by DoE last year as part of a general reduction of funding in the EOR related research areas. We will therefore focus in the coming year solely on finishing the projects listed as part of year 2 in our proposal.

Relaxation schemes

The main conclusions of this work are:

- The constant sub-characteristic Jin-Xin scheme is attractive for two-phase multicomponent systems in that it removes the dependency of the numerical solver on the eigenstructure of the system and nonlinear Riemann solutions. But, the necessary restriction on the sub-characteristic speed results in excessive numerical diffusion that can significantly reduce solution accuracy in strongly nonlinear compositional problems.

- The new constant $\alpha - \beta$ system does not offer sufficient improvement and behaves like the Jin-Xin scheme for eigenvalues with equal magnitude, or the corresponding upwind schemes when small negative eigenvalues are present.

- The variable version of the Jin-Xin relaxation maintains all the advantages of standard the Jin-Xin scheme, while reducing numerical diffusion considerably by locally imposing the sub-characteristic condition. For ternary gas-oil displacement system, our extensive testing showed that in many cases the second order variable relaxation scheme is

competitive with component-wise ENO-RK3 and that it is always as least as good as component-wise TVD-RK2.

- Variable $\alpha - \beta$ relaxation, where all eigenvalues are chosen to closely follow the physical speeds of the system, will result in an ill-conditioned problem. A better alternative is to vary only the positive eigenvalues of the $\alpha - \beta$ relaxation system, while keeping the negative eigenvalues close to $-f'_{max}$. This results in a scheme with performance similar to variable Jin-Xin relaxation.

References

Aregba-Driollet D, Natalini R. 1996. ”Convergence of relaxation schemes for conservation laws.” *Appl Anal.* 61:163-193.

Banda MK. 2005. Variants of relaxed schemes and two-dimensional gas dynamics. *J. Comp. Appl. Math.* 175:41-62.

Batycky RP, Blunt M, Thiele MR. 1997. A 3D field-scale streamline based reservoir simulator *Soc. Petrol. Eng. Res. Eng.* 12:246-254.

Chalabi A. 1999. Convergence of relaxation schemes for hyperbolic conservation laws with stiff source terms. *Math. Comput*. 68:955-970.

Chapman S, Cowling TG. 1970. *The Mathematical theory of nonuniform gases*. Cambridge Univ. Press.

Delis AI, Katsounis Th. 2005. Numerical solution of the two-dimensional shallow water equations by the application of relaxation methods. *Appl. Math. Mod*. 29(8): *754-783.*

Dindoruk B. 1982. *Analytical theory of multiphase, multicomponent displacement in porous media*. PhD thesis. Stanford Univ.

Gerritsen M, Durlofsky LJ. 2005. Modeling fluid flow in oil reservoirs. *Annu. Rev. Fluid Mech*. 37:211-238.

Harten A, Engquist B, Osher S, Chakravarthy S. 1987. Uniformly high order accurate essentially non-oscillatory schemes III. *J. Comp. Phys*. 71:231–303

Hundsdorfer W, Verwer JG. 2003. *Numerical solution of time-dependent advection-diffusion-reaction equations*. Springer Series in Comp. Math.

Jessen K, Wang Y, Ermakov P, Zhu J, Orr FM Jr. 2001. Fast, approximate solutions for 1D multicomponent gas injection problems. *Soc. Petrol. Eng. J.* 6(4):442–451.

Jessen K, Orr FM Jr. 2002. *Compositional streamline simulation*. Presented at the SPE Annu. Tech. Conf. Ex., San Antonio, Texas

Jessen K, Stenby EH, Orr FM Jr. 2004. Interplay of phase behavior and numerical dispersion in finite difference compositional simulation. *Soc. Pet. Eng. J.* 9(2):193-201

Jin S. 1995. Runge-Kutta methods for hyperbolic conservation laws with stiff relaxation terms. *J. Comp. Phys.*122:51-67.

Jin S, Xin ZP. 1995. The relaxation schemes for systems of conservation laws in arbitrary space dimensions. *Comm. Pure Appl. Math*. 48:235-277.

Jin S, Katsoulakis MA. 1997. Relaxation approximations to front propagation. *J. Diff. Equations*. 138:380-387.

Jin S, Xin ZP. 1998. Numerical passage from systems of conservation laws to Hamilton-Jacobi equation, and a relaxation scheme. *SIAM J. Num. Anal*. 35:2385-2404.

Juanes R, Patzek TW. 2004. Relative permeabilities for strictly hyperbolic models of three-phase flow in porous media. *Trans. Porous Med.* 57:125–152

Kurganov A, Tadmor E. 2000. New high-resolution central schemes for nonlinear conservation laws and convection-diffusion equations. *J. Comp. Phys.*160:241-282.

Lake LW. 1989. *Enhanced Oil Recovery*. Englewood Cliffs, NJ: Prentice-Hall.

LeVeque RJ. 2002. *Finite volume methods for hyperbolic problems*. Cambridge texts Appl. Math.

LeVeque RJ, Pelanti M. 2001. A class of approximate Riemann solvers and their relation to relaxation schemes. *J. Comp. Phys.* 172:572-591.

Liu HL, Warnecke G. 2000. Convergence rates for relaxation schemes approximating conservation laws. *SIAM J. Num. Anal*. 37:1316-1337.

Liu TP. 1987. Hyperbolic conservation laws with relaxation. *Comm. Math. Phys.*108:153:175.

Lohrenz J, Bray BG, Clark CR. 1964. The viscosity of pure substances in dense liquid and gaseous phases. *J Petrol. Technol.* 1:1171-1176

Mallison BT, Gerritsen MG, Jessen K, Orr FM Jr. 2003. *High order upwind schemes for twophase multicomponent flows*. Presented at the Soc. Petrol. Eng. Res. Sim. Symp., Houston, Texas

Mallison BT. 2004. *Streamline-based simulation of two-phase, multicomponent flow in porous media.* PhD thesis. Stanford Univ.

Nessyahu H, Tadmor E. 1990. Non-oscillatory central differencing for hyperbolic conservation laws *J. Comp. Phys.*87(2):408-463.

Orr FM Jr., Dindoruk B, Johns RT. 1995. Theory of multicomponent gas/oil displacements. Ind. Eng. Chem. Res. 34:2661–2669.

Orr FM Jr. 2005. *Theory of Gas Injection Processes*. Stanford Univ.

Qiu J, Shu CW. 2002. On the construction, comparison, and local characteristic decomposition for high order central WENO schemes. *J. Comp. Phys.* 183(1):187–209

Sweby PK. 1984. High resolution schemes using flux limiters for hyperbolic conservation laws. *SIAM J. Num. Anal*. 21:995–1011

Tadmor E, Tang T. 2001. Pointwise error estimates for relaxation approximations to conservation laws. *SIAM J. Math. Anal*. 32:870-886.

Van Leer B. 1979. Towards the ultimate conservative difference schemes V: A second order sequel to Godunov's method *J. Comp. Phys.*32:101-136.

Younis R, Gerritsen M. 2006. *Multiscale process coupling by adaptive fractional stepping: An in-situ combustion model*. Presented at the Soc. Petrol. Eng. Symp. on Improved Oil Recovery, Tulsa, Oklahoma.

Figures

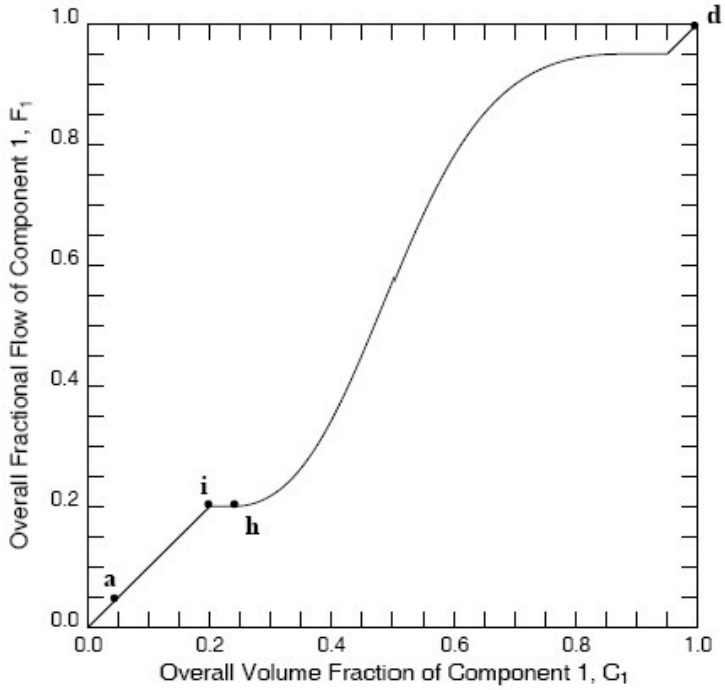

Figure 1: Fractional flow function $F_1(C_1)$. In the two-phase region, the function is S-shaped.

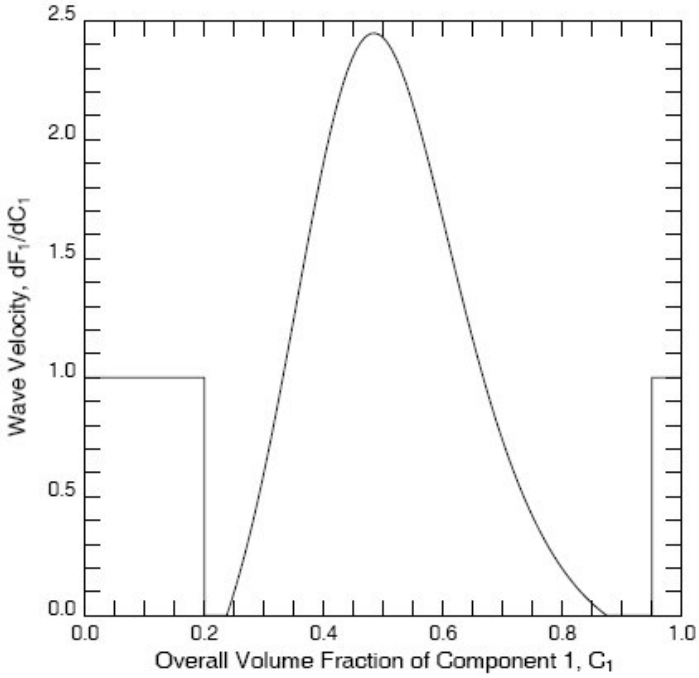

Figure 2: Derivative $\frac{dF_1}{dC_1}$ of the fractional flow function shown in figure 1.

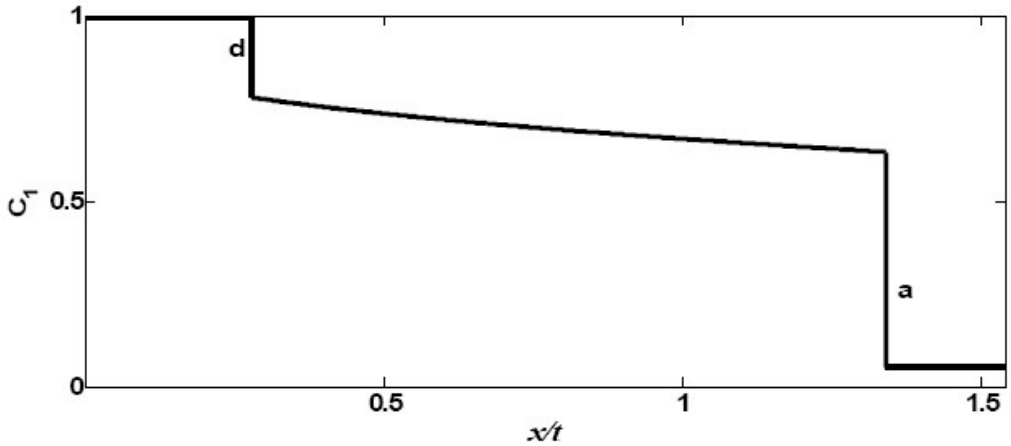

Figure 3: Binary displacement – test case 1, pure light component (**d**) displaces pure heavy component (**a**).

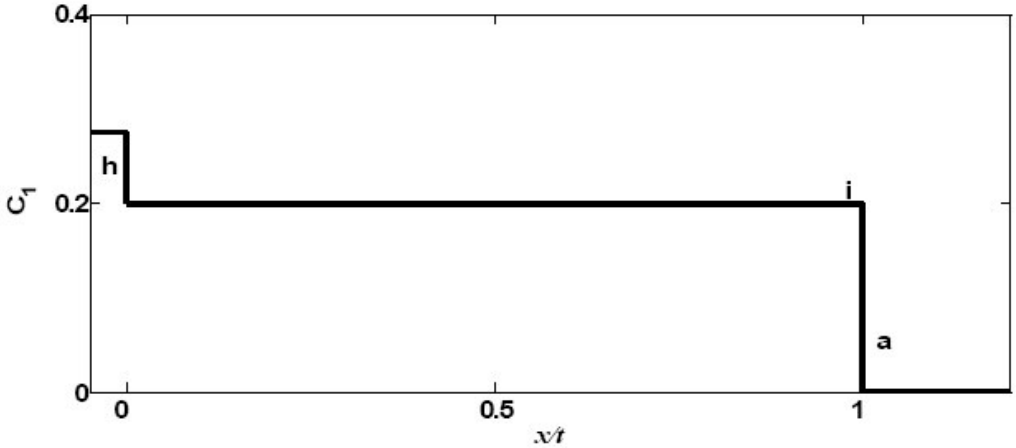

Figure 4: Binary displacement - test case 2, mixture of two components (**h**) displaces pure component (**a**). The trailing shock has zero speed.

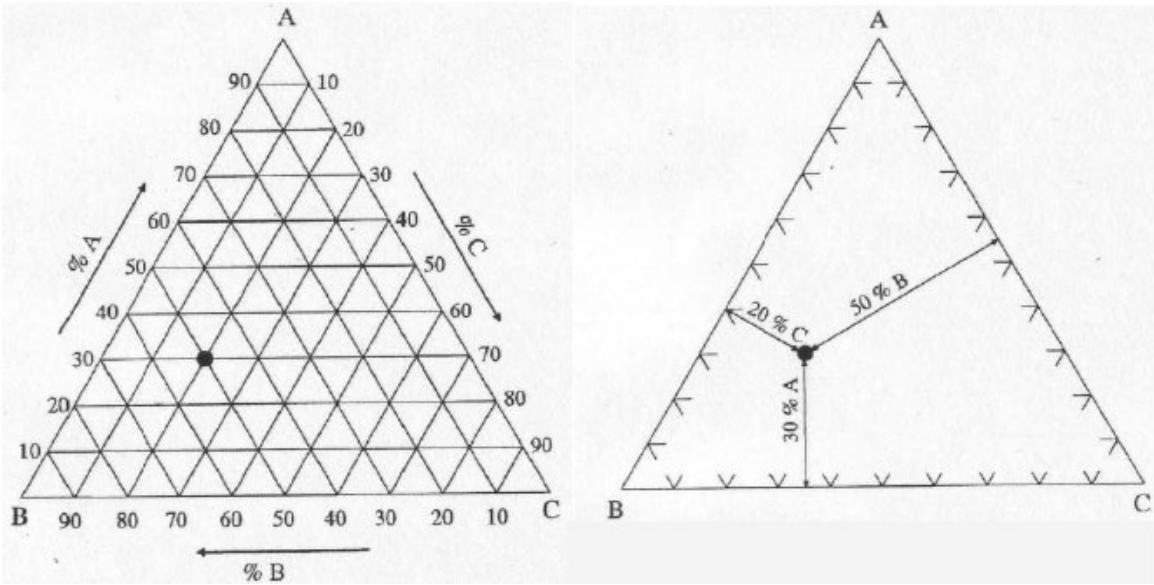

Figure 5: Ternary phase diagram - representation of a ternary composition on an equilateral triangle.

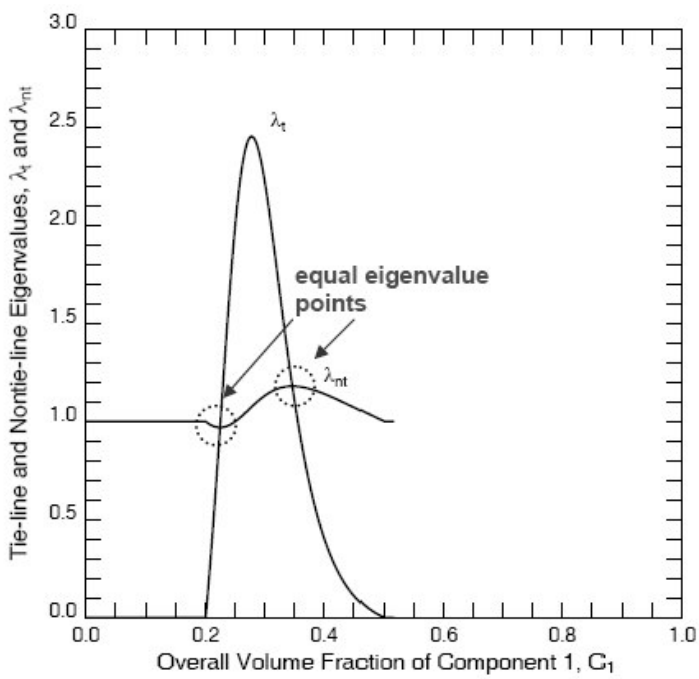

Figure 6: Tieline and non-tieline eigenvalues.

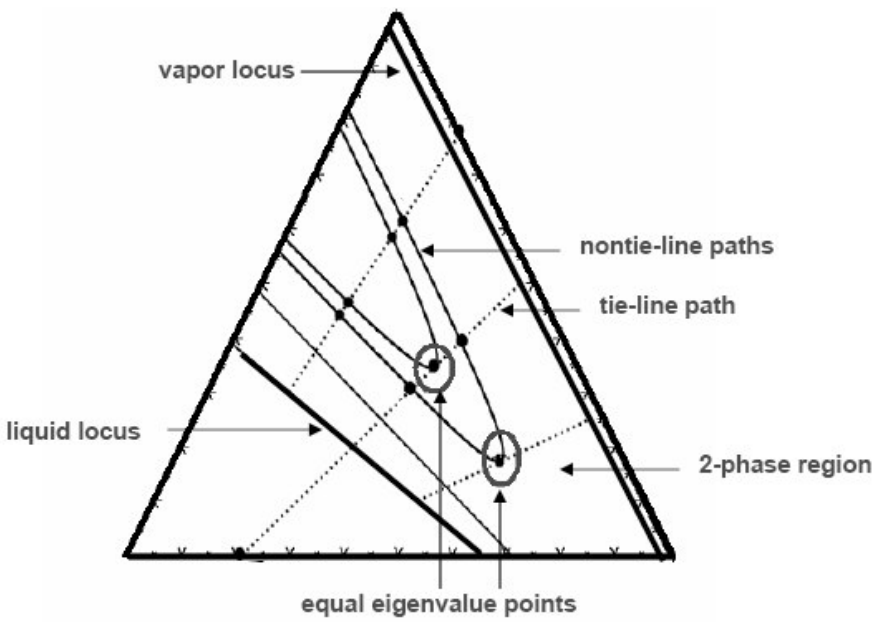

Figure 7: Tie-line and nontie-line paths for a ternary system with constant K-values. At equal eigenvalue points, the nontie-line path is tangent to tie-line path.

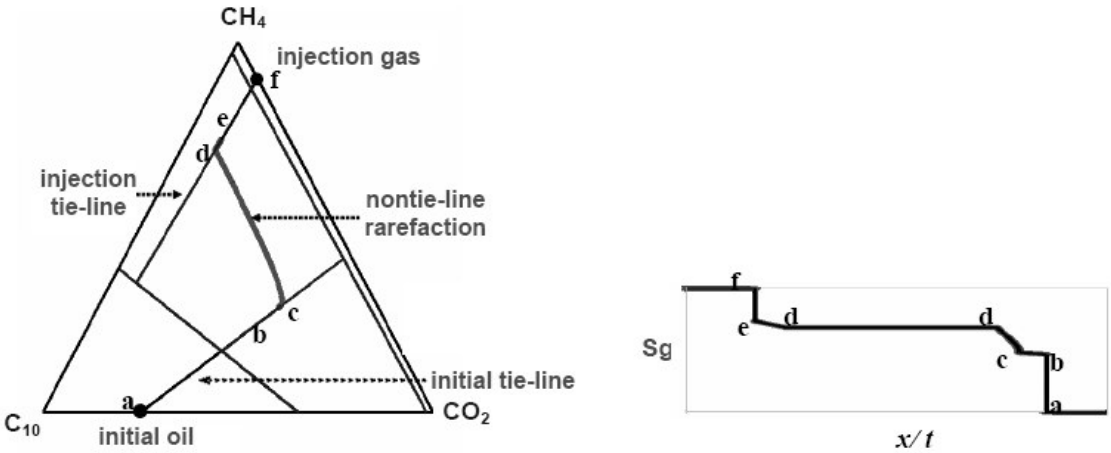

Figure 8: Solution path in the ternary phase diagram and saturation profile of the 3-component displacement.

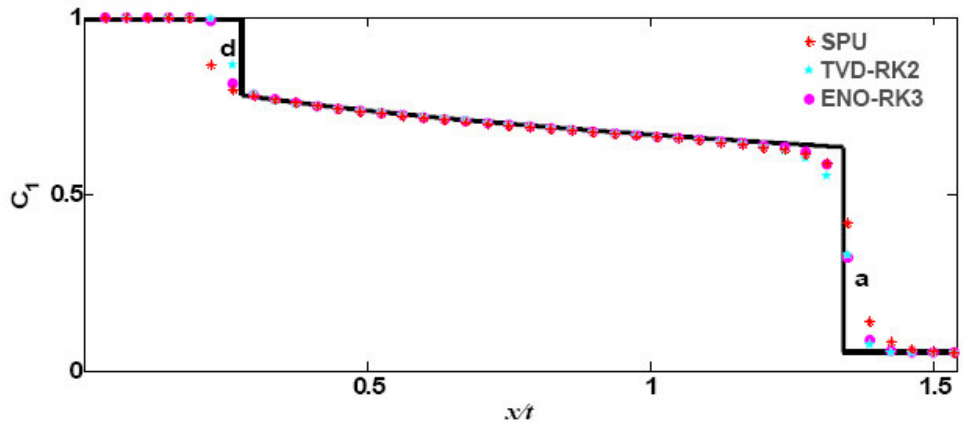

Figure 9a: Results of upwind schemes on test case 1- binary displacement. N= 40, CFL = 0.35.

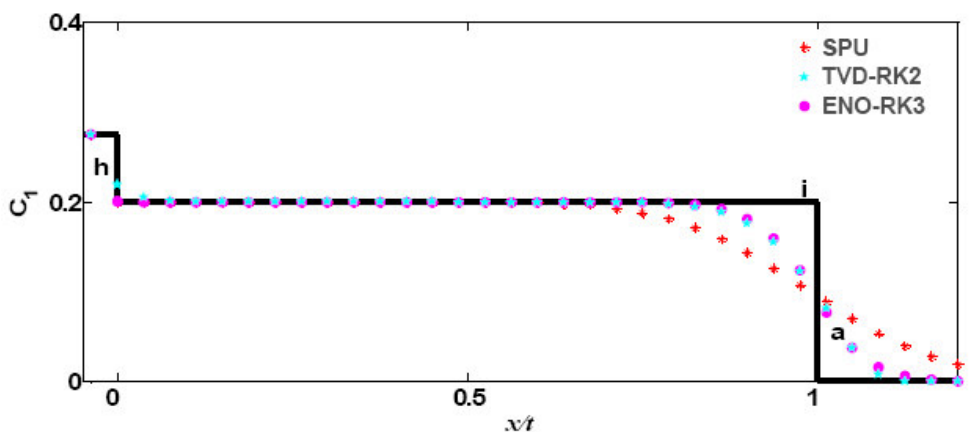

Figure 9b: Results of upwind schemes on test case 2- binary displacement. N= 40, CFL = 0.35. Here, the SPU needs about 200 grid points to resolve as accurately as TVD-RK2 or ENO-RK3.

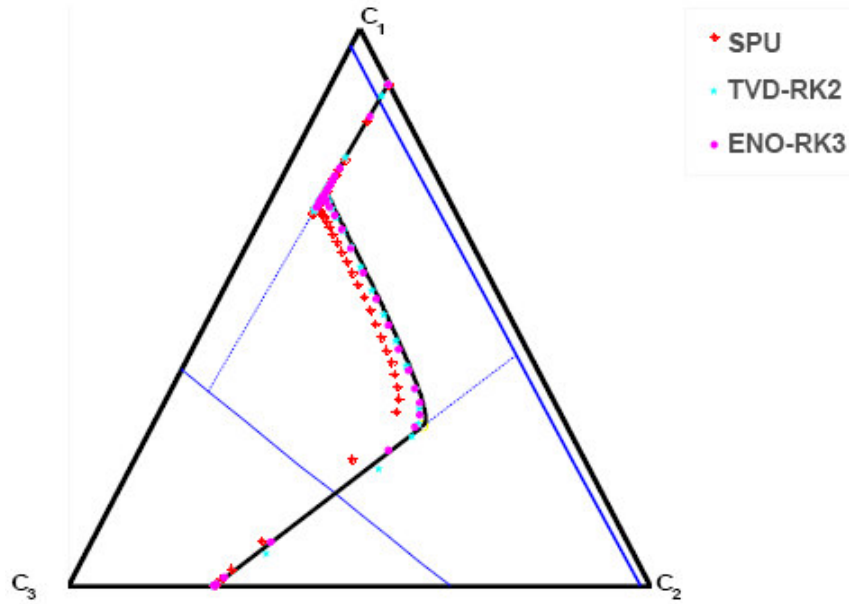

Figure 10a: Results of component-wise application of upwind schemes on ternary displacement in the phase space . SPU is excessively diffusive. N= 80, CFL = 0.4.

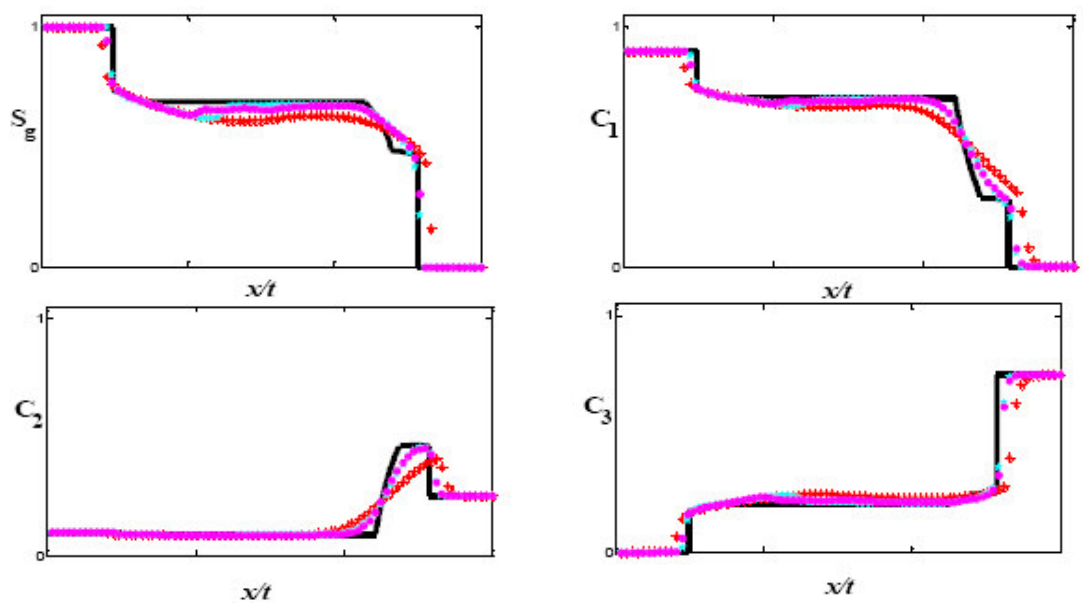

Figure 10b: Solution profiles of ternary displacement got by component-wise application of upwind schemes. SPU smears the shocks and has a prominent dip in the zone-of-constant state. N= 80, CFL = 0.4.

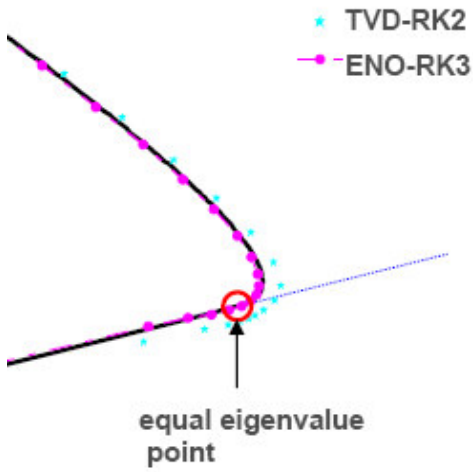

Figure 11: A closer look at the TVD-RK2 and ENO-RK3 composition paths in the phase space, near the equal eigenvalue point. The path computed by the TVD-RK2 scheme jumps to an incorrect nontie-line near the equal eigenvalue point. N= 200, CFL = 0.4.

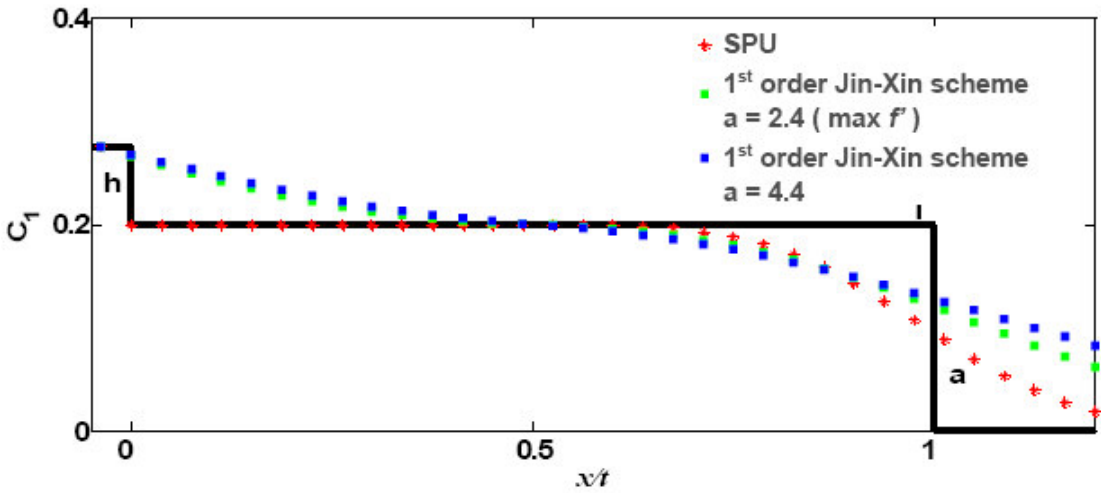

Figure 12: Comparison of 1st order Jin-Xin relaxation scheme and SPU. N= 40, CFL = 0.2.

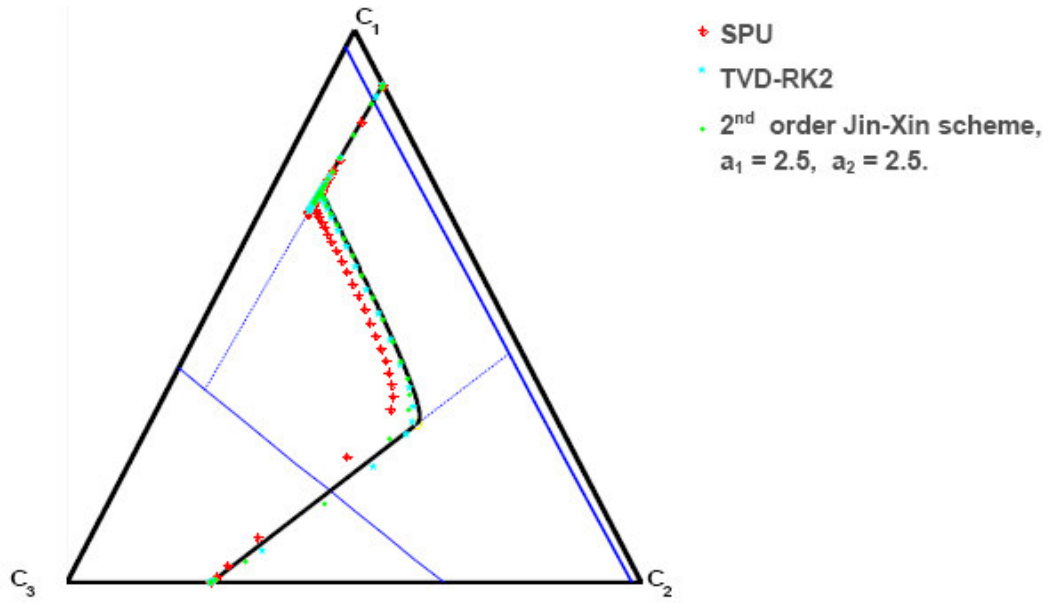

Figure 13a: Phase space comparison of component-wise application of upwind schemes and 2nd order Jin-Xin relaxation scheme on ternary displacement. Composition path of Jin-Xin scheme is close to TVD-RK2 but has slightly more numerical diffusion than TVD-RK2. N= 80, CFL = 0.2.

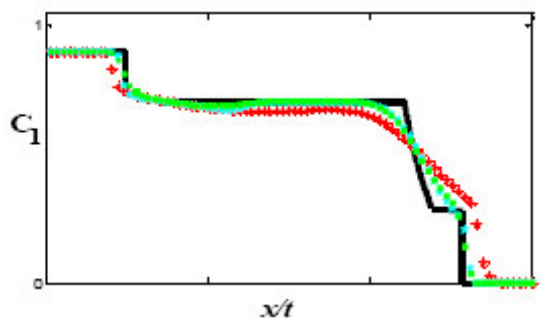

Figure 13b: Solution profile of C_1 obtained by 2nd order Jin-Xin relaxation scheme is close to TVD-RK2. N= 80, CFL = 0.2.

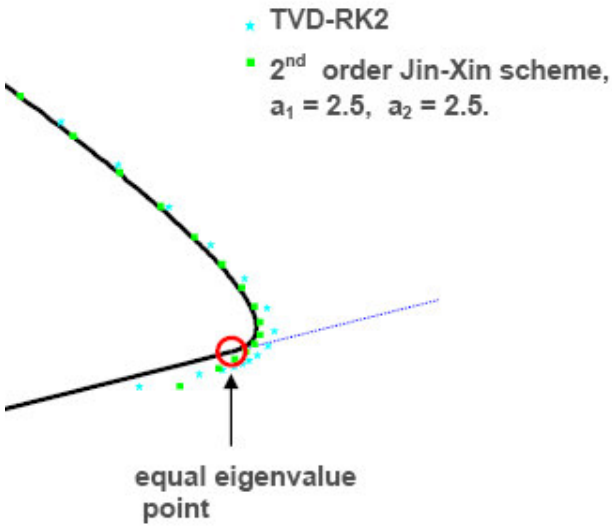

Figure 14: A closer look at the 2nd order Jin-Xin scheme in the phase space near the equal eigenvalue point. The path computed by the Jin-Xin scheme behaves better than TVD-RK2 near the equal eigenvalue point but also has slightly more diffusion on the initial tie-line. N= 200, CFL = 0.2.

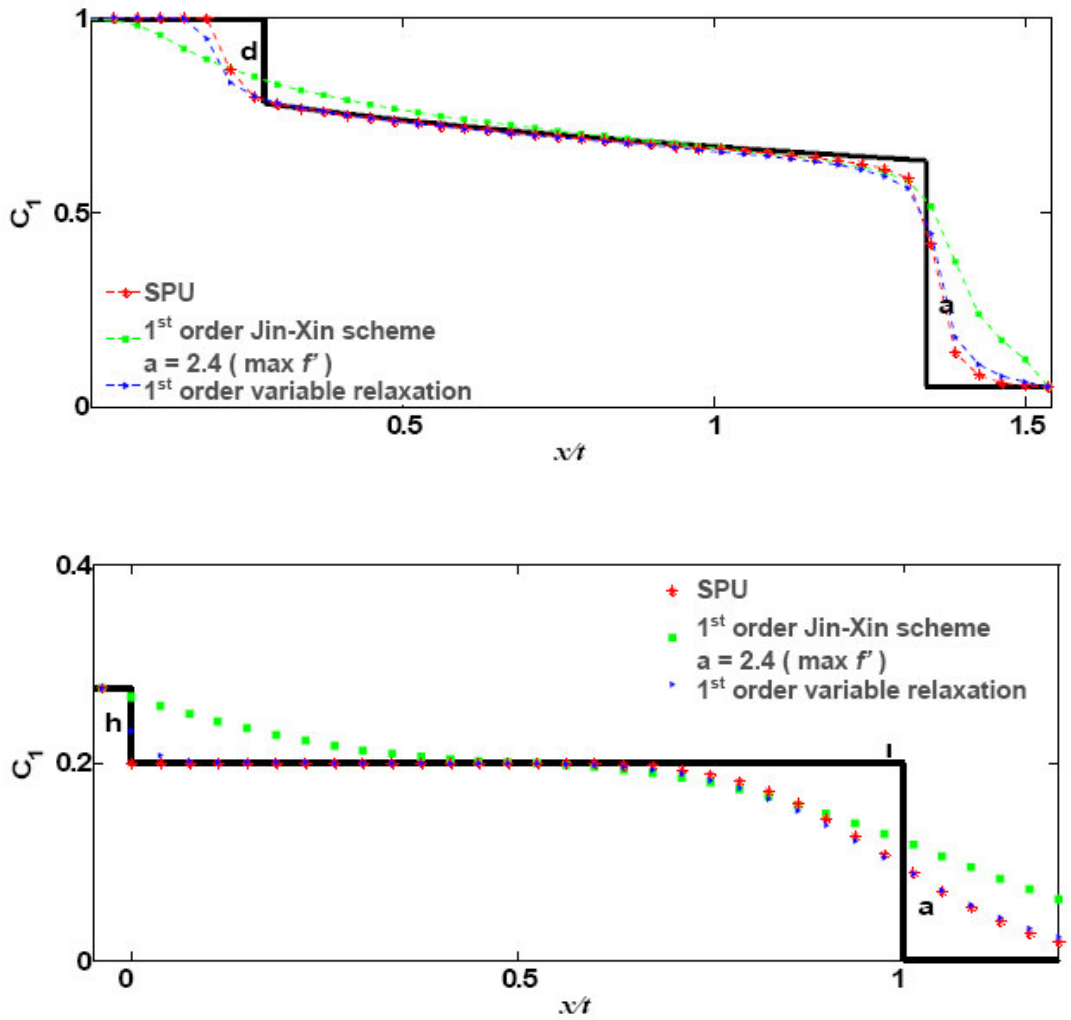

Figure 15a & 15b: Results of variable relaxation scheme on binary displacement. N= 40, CFL = 0.35. Variable relaxation scheme is less diffusive than Jin-Xin scheme and is quite close to SPU.

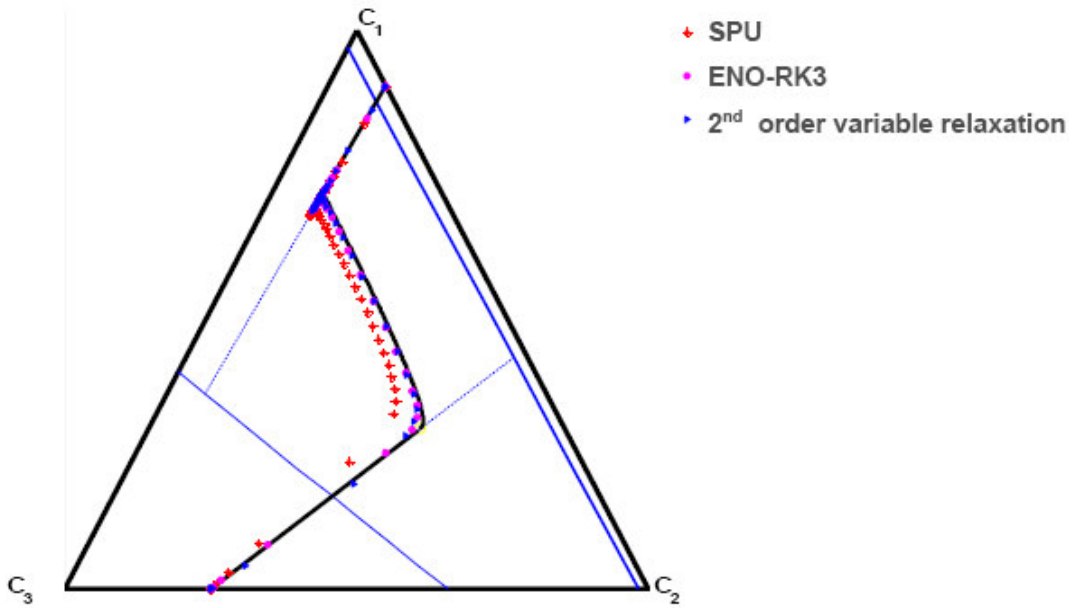

Figure 16a: Phase space comparison of ENO-RK3 and 2nd order variable relaxation scheme on ternary displacement. Composition path of the variable relaxation scheme is close to ENO-RK3. N= 80, CFL = 0.2.

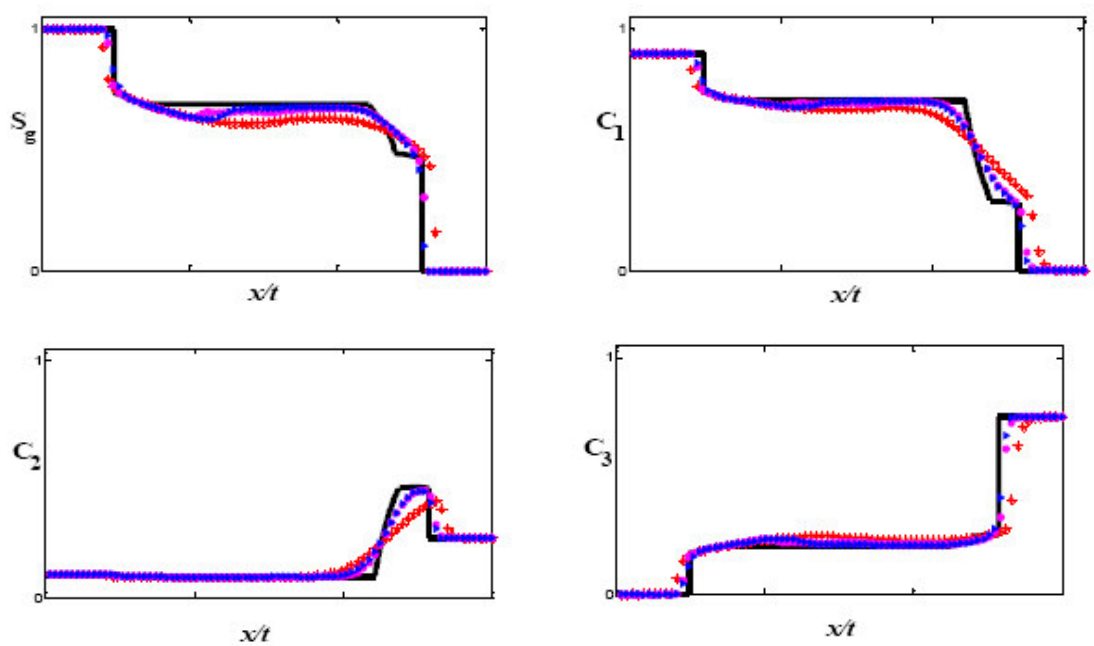

Figure 16b: Comparison of solution profiles obtained by ENO-RK3 and 2nd order variable relaxation. N= 80, CFL = 0.2.

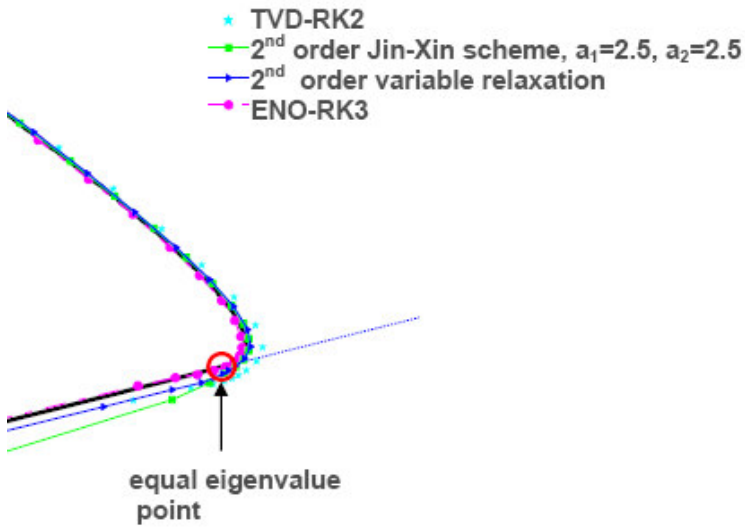

Figure 17: A closer look - 2nd order variable relaxation is close to ENO-RK3 and has much less diffusion than Jin-Xin scheme. It also behaves well near the equal eigenvalue point. N= 200, CFL = 0.2.